


國立交通大學

光電工程研究所

碩士論文

飛秒光參數放大器及其特性研究



**Construction and Characterization  
of Femtosecond Optical  
Parametric Amplifiers**

研究生：黃龍進

指導教授：潘犀靈 教授

中華民國九十三年七月

# 飛秒光參數放大器及其特性研究

## Construction and Characterization of Femtosecond Optical Parametric Amplifiers

研究生：黃龍進

Student: Ling-Chin Huang

指導教授：潘犀靈 教授

Advisor: Prof. Ci-Ling Pan

國立交通大學

光電工程研究所



A Dissertation

Submitted to Institute of Electro-Optical Engineering  
College of Electrical Engineering and Computer Science  
National Chiao Tung University

In partial Fulfillment of the Requirements

for the Degree of

Master of Engineering

In

Electro-Optical Engineering

August 2004

Hsinchu, Taiwan, Republic of China

中華民國九十三年八月

# 國立交通大學

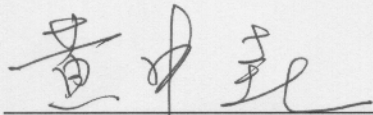
## 論文口試委員會審定書

本校光電工程研究所碩士班 黃龍進 君

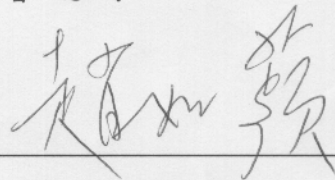
所提論文 光參數放大器及其特性研究

合於碩士資格標準、業經本委員會評審認可。

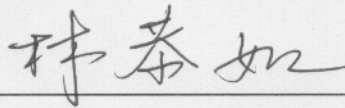
口試委員：



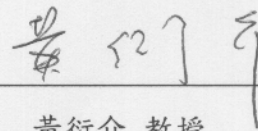
黃中堯 教授



趙如蘋 教授



林恭如 教授



黃衍介 教授

指導教授：



潘犀靈 教授

所長：



教授

賴暎杰 教授

中華民國九十三年七月十九日

# 飛秒光參數放大器及其特性研究

研究生：黃龍進

指導老師：潘犀靈 教授

國立交通大學光電工程研究所

## 摘要

利用在晶體內產生的二階非線性機制(光參數放大, OPA)去架設一套波長可調的雷射, 並且利用頻率解析光時閘(FROG)的技術去量測脈衝的特性。藉由調整 BBO 的角度, 滿足相位匹配的波長就會被放大, 而範圍從 1141 到 1524 奈米; 而同時另一道因滿足能量守恆的波長也會被產生出來, 範圍從 1684 到 2677 奈米。輸出光源的平均功率大約有數十個 mW, 而脈衝寬度大約 50 飛秒。

另一部份, 我們參考利用多道光源去做光參數放大以及非共線光參數放大, 另外還引進 single-shot 的幾何結構去做超寬頻的光參數放大。為了了解這些變數在這樣的過程中有著怎樣的影響, 就去做了一連串相關的實驗去了解到這些參數在這非線性過程中會有怎樣的影響。藉由這一連串的實驗, 具有 300 奈米頻寬的脈衝可以藉由這樣簡單的技术被放大產生出來。倘若這個脈衝經由適當的元件去壓縮, 他的脈衝寬度期望可以到達 2.4 飛秒的等級。

# Construction and Characterization of Femtosecond Optical Parametric Amplifiers

Student: Lung-chin Huang

Advisor: Prof. Ci-Ling Pan

Institute of Electro-Optical Engineering  
College of Electrical Engineering and Computer Science  
National Chiao Tung University

## Abstract

We construct and characterize a femtosecond (fs) 800nm pumped BBO type II collinear optical parametric amplifier (OPA) nonlinear crystal. By tuning the phase matching angle of the BBO crystal, we could obtain the output from 1141 to 1524 nm for the signal beam. The idler tuning range is expected to be 1684 to 2677 nm. The characterizations of this system were that the average output power could be several tens of mW and the pulse duration was estimated to be around 50fs.

Additionally, we employ the multi-beam pump, noncollinear optical parametric amplification and the single-shot geometric scheme to generate the amplified light with ultra-broad bandwidth. To understand the mechanism about this process, we attempt to know what the effect of each variable is. From these results, the pulses with bandwidth over 300 nm are generated by this simple technique and the duration of 2.4 fs is expected after the suitable compressor.

## Acknowledgement (致謝)

在研究所課程學習的每個過程中都有它有趣與好玩的地方，尤其是實驗的部分，許多書中所提到的現象能實際呈現在眼前時，是最令人感到興奮的時候。雖然在最後加緊腳步做實驗和分析數據時相當累人，但是整體而言，這是一趟結果令人欣慰與滿意的學習旅程。其中，有許多親友及師長陪我一起渡過這段辛苦卻快樂的日子，對此，要獻上我對他們無比的感謝。

我最要感謝的人是我的爸爸，他給予我經濟上的支助以及生活上的幫助，讓我可以無後顧之憂地用全部精神去完成我的論文及研究；此外，雖然我的媽媽很早就已經去逝，但是感謝她辛苦地把我生下來，讓我可以有機會享受並一窺這個世界，真的非常謝謝我的爸媽，讓我可以在這個世界上盡情地遊玩、觀賞和學習；另外，感謝我的四個姊姊以及親戚們，不時地給予我生活上的協助，讓我在生活中的困難之處得以順利解決，並持續朝我的目標邁進。

在我研究所學習及研究的路途上，則非常感謝我的指導教授 潘犀靈教授，給予我學業及論文上的指導和幫助。另外還要感謝子安、晁達、晉瑋、怡超學長及玉屏學姐在實驗及觀念上的指正，化解了我研究學習上的困惑與阻礙。還有已畢業的碩班學長們，宗盛、世軒、建宏、威宏和嗣文，讓我剛進實驗室時對實驗有初步的瞭解，給予我研究上的經驗傳授。另外，因為有我的同學，秉其、之揚、學智、沛霖和奕帆大家彼此間互相扶持學習，讓我順利完成碩士論文；學弟照仁、羅誠、弘倫、冠文、禎佑、沁融和宗翰破除了過程中的枯燥與乏味，也讓我愉快地渡過最後這段研究的日子。

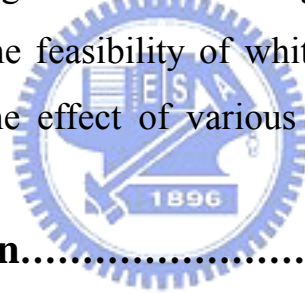
最後我要感謝一個特別的人，很幸運地，在這段研究的過程中，我認識了我的女朋友。在這最辛苦的日子裡，感謝她的陪伴帶給我快樂的時光，讓我的身心得以喘息，並且再度獲得向前邁進的動力。

黃龍進 于 風城 交大 九十三年八月

# Contents

	Page
<b>Chinese Abstract</b> .....	<b>i</b>
<b>English Abstract</b> .....	<b>ii</b>
<b>Acknowledgement</b> .....	<b>iii</b>
<b>Contents</b> .....	<b>iv</b>
<b>Chapter I Introduction</b> .....	<b>1</b>
1.1 The Ultrafast Laser.....	1
1.2 Toward the Few-Cycle Laser by Nonlinear Mechanism.....	3
1.3 Tunable Laser.....	6
1.4 Motivation and Objective.....	12
1.5 Organization of this thesis.....	12
<b>Chapter II Theory</b> .....	<b>13</b>
2.1 Basic Theory of Optical Parametric Amplification.....	13
2.1.1 Introduction of Optical Parametric Amplification.....	13
2.1.2 Coupled-wave Equation.....	15
2.1.3 Effective Lengths.....	17
2.1.4 Optical Parametric Amplification Process for Non-ultrashort Pulses.....	18
2.1.5 Optical Parametric Amplification Process for Ultrashort Pulses.....	19
2.1.6 Important Parameters for Ultrafast OPA.....	20
2.2 Theory of Broadband Optical Parametric Amplification.....	27
2.2.1 Non-collinear visible Optical Parametric Amplification .....	27

2.2.2	Two-beam Pump (Multi-beam pump) OPA.....	29
2.2.3	Single Shot Geometric Scheme.....	31
2.2.4	White Light OPA.....	32
<b>Chapter III Collinear Optical Parametric Amplifiers.....</b>		<b>37</b>
3.1	Experimental System Configuration.....	37
3.2	Result of Collinear Optical Parametric Amplifiers.....	41
<b>Chapter IV White Light Optical Parametric Amplifiers.....</b>		<b>48</b>
4.1	Experimental System Configuration.....	48
4.2	Result of the White Light Optical Parametric Amplifiers....	50
4.2.1	Tuning Range at Various $\alpha$ Angle.....	50
4.2.2	Verifying the feasibility of white light OPA.....	53
4.2.3	Studying the effect of various parameters.....	55
<b>Chapter V Conclusion.....</b>		<b>60</b>
5.1	Summary.....	60
5.2	Future Directions.....	61
<b>Reference.....</b>		<b>62</b>

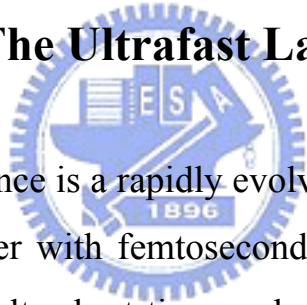




# Chapter I Introduction

Over the past decades, techniques for the production and manipulation of short optical pulses have progressed at an accelerated rate, reducing the time interval accessible to measurements from the millisecond ( $10^{-3}$  sec) in ~1949 to the femtosecond ( $10^{-15}$  sec) regime in ~1985. Recently, the nonlinear mechanism is used to reduce the pulse duration and to tune the wavelength of the pulse. In this chapter, I make a brief description of generating the few-cycle pulse and tuning the wavelength by taking advantage of the nonlinear mechanism.

## 1.1 The Ultrafast Laser [1]



Ultrafast optical science is a rapidly evolving multidisciplinary field: the ability to excite matter with femtosecond light pulses and probe its subsequent evolution on ultrashort time scales opens up completely new fields of research in physics, chemistry, and biology. Furthermore, the high intensities that can be generated using femtosecond light pulses allow us to explore new regimes of light-matter interaction. The implementation of more sophisticated spectroscopic techniques has been accompanied by improvements in laser sources. Considerable effort has been dedicated to the achievement of shorter light pulses, to improve temporal resolution; other efforts have worked to expand the frequency tunability of the pulses.

The 1990s have witnessed a revolution in ultrafast laser technology, thanks to the advent of solid state active materials, such as Ti: sapphire,

and powerful mode-locking techniques, such as Kerr lens mode locking (KLM). With these advances, femtosecond lasers have gained tremendously in reliability and user-friendliness. Another landmark of femtosecond technology has been the chirped pulse amplification (CPA) technique, which enabled increasing the energy of femtosecond lasers by 2–3 orders of magnitude, from the millijoule to the multijoule level. This increase in peak power makes it possible to access a whole new class of nonlinear optical phenomena, triggering a renaissance in the field of nonlinear optics. Parallel to these developments has been the discovery of novel nonlinear optical crystals, such as b-barium borate (BBO) and lithium triborate (LBO), combining improved optical characteristics (high nonlinear optical coefficients, low group velocity dispersion, broad transparency ranges) with high damage thresholds.

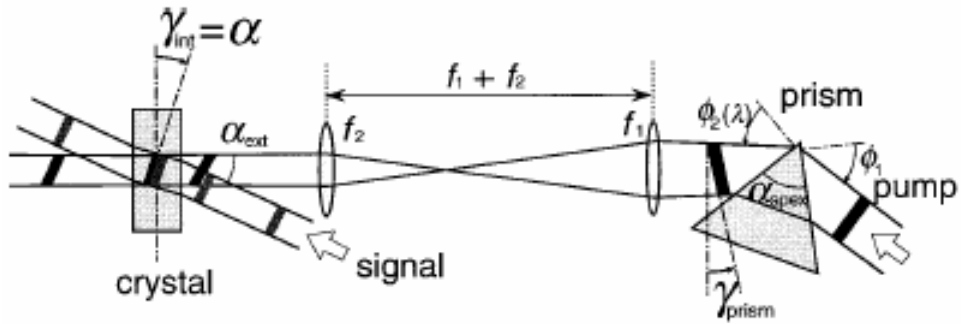


## 1.2 Toward the Few-Cycle Laser by Nonlinear Mechanism

To generate ultrashort pulse, a broad bandwidth is required. It is desirable to utilize the nonlinear mechanism to make the different wavelength amplified simultaneously. The suitable devices that could compensate its group velocity dispersion are using to compress the generated pulses. Then, the few-cycle laser could be generated from these processes. Since we make use of optical parametric generation of second-order nonlinear effect to produce the broad bandwidth beam, the energy and momentum conservation of the interacted beams in the nonlinear mechanism must be satisfied. The momentum conservation (phase matching condition) is related to the generated wavelength of the amplified seeding beam. We could make the various wavelengths (over broad bandwidth) satisfy the two laws at the same time by using the geometric issues. Recently, there are many methods to be demonstrated. These methods include (1) Noncollinear Optical Parametric Amplification (NOPA) [2]; (2) Pulse-Front-Matched OPA [3, 4]; (3) Two beam pump OPA (further multi-beam pump) [5]; (4) Chirped-Pulse Optical Parametric Amplifier (CPOPA) with angularly dispersed beams [6]; (5) white light OPA. Here I briefly describe these methods. The detail about the method (1), (3) and (5) is explained in the next chapter.

Because the bandwidth of the generated OPA pulses could be broadened by reducing the group velocity mismatch (GVM) between the signal and the idler. Since the optical parametric amplification is three-wave mixing of the second order nonlinearity including the pump, the seeding (signal) and the idler, NOPA means that the pump beam hits

the nonlinear crystal at an angle with respect to the signal. In such a scheme, the GVM could be decreased and the bandwidth is broadened. For the pulse-front matched of the pump and the signal, the wave-front of the pump is tilted by a prism and a telescope to match the one of the signal inside the nonlinear medium, seeing the Fig. 1-1. Because the GVM could be reduced through this process, the amplified signal can have the broader bandwidth. The other way is that several individual bandwidths with different central wavelength are combined and the total effective bandwidth could be broadened. If there are several-beams pump in an OPA system, the different wavelength due to different phase matching condition resulted from the different pump beam is amplified simultaneously. The effective bandwidth could be broadened because of combining the several individual bandwidths. The two-beam pump OPA uses this concept and the effective bandwidth combining the two individual bandwidths is quiet broader than the bandwidth with single pump beam. The fourth method is similar as the two-beam pump. It takes advantage of the pulse-front matched and the signal with angularly dispersed beams to make different wavelength be amplified simultaneously. The white light OPA integrates the NOPA and the two-beams pump OPA to generate the ultrabroadband pulse. The single-shot geometry [7] is used to compensate the temporal overlap. The Table 1-1 states the characterizations various few-cycle lasers.



Source: T. Kobayashi, Appl. Phys. B v70, s239(2000)

Fig. 1-1 The scheme of the pulse-front-matching device

Method	Wavelength (nm)	Bandwidth (THz)	Transform Limit (fs)	Duration after compressor(fs)	Reference
(1)	535-790	180	6.5	7.2	[2]
(1)+(2)	550-775	200	4.4	4.7	[3],[4]
(3)	720 (center)	11.6	38	61	[5]
(4)	600-1200	200	5.2		[6]
(5)	510-840	217	2.0		

Table 1-1 The bandwidth and the pulse width of various broad-band laser

## 1.3 Tunable Laser

Since high power, ultrafast laser pulses with tunable frequency over a wide spectral range from the ultraviolet (UV) to the infrared (IR) would make it possible to excite in resonance different materials and to probe optical transitions occurring at different frequencies, its applications contain many field: physics, astronomy, spectroscopy, isotope separation, materials research and development, remote sensing, and medicine. For example, it can be used in time-resolved spectroscopy to yield new information about fundamental properties of materials, to identify transient species, to characterize new nonlinear optical materials, and to study the dynamics of optoelectronic systems. Early tunable sources of femtosecond optical pulses were based on dye laser technology and mode-locked solid state laser, but they only provide the pulses in the visible and near infrared region with limited tuning ranges. In dye laser, some frequency tunability could be achieved by simply changing the laser dye. This flexibility, however, came at the expense of a complicated and time consuming reoptimization. In addition, because of the lack of suitable laser media, the mid-IR laser pulses are difficult to generate.

In the last years, the various tunable lasers are developed over the pulsed regime (dye laser, Ti: Sapphire laser...), continuous wave regime (semiconductor lasers), and line-tunable CW lasers (ArF, KrF, XeF...). Here, I would state the different laser in the pulsed regime. The following table is Emission Characteristics available from broadly tunable sources of coherent radiation in the pulsed regime.

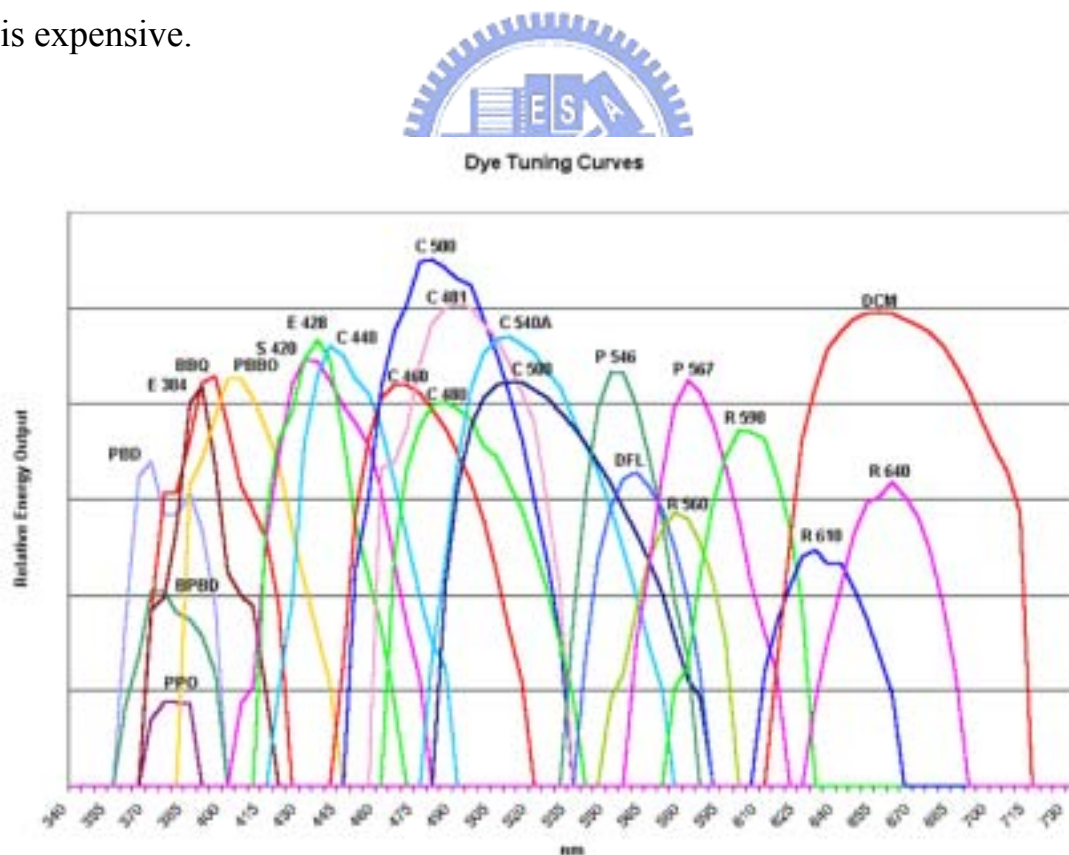
Tunable source	Spectral range	Energy	Average power
Dye laser	320-1200 nm	400 J	2.5 kW at 13.2 kHz
Ti: Sapphire laser	660-986 nm	6.5 J	5.5 W at 6.5 kHz 220 W at 110 Hz
Cr <sup>3+</sup> : BeAl <sub>2</sub> O <sub>4</sub> laser	701-818 nm	>100 J	
Optical parametric oscillators based on BBO	0.41-2.7	>100 mJ	
Free-electron lasers	2 μm-1 mm		> 10W

Table 1-2 wavelength coverage available from pulsed broadly tunable sources of coherent radiation [8]

The following statements focus mainly on the tunable laser accomplished by using nonlinear optical effects that can be employed for frequency conversion. But before I describe the tunable laser by nonlinear mechanism, I want to review the prior tunable laser in the pulsed regime. First, the dye lasers are described. The dye lasers offer the broad tunability from the near ultraviolet to the near infrared (Fig. 1-2), facilitated by way of the existence of hundreds of laser dye molecular species. Then, I briefly introduce the solid state laser for various gain medium. Besides, the characterizations of the tunable wavelength of the Free Electronic Lasers are described. Finally, I state the tunable laser by using the nonlinear mechanism, such as optical parametric amplification (OPA) and optical parametric oscillation (OPO).

## Dye Laser

In 1966, the dye lasers were constructed by Sorokin. If any mode-locking mechanism, the dye lasers are cw mode. After adding the mode-locking device, the dye lasers become the pulsed laser. But according to the various dyes, the dye lasers are operated under the pulsed mode and the cw mode. And the characterizations of the dye lasers depend on the different dyes, such as cyanine, merocyanine...etc. See the Fig. 1-2, there is the coverage wavelength response for the different dyes. For the other wavelength region, the dyes must be changed. Although the dye lasers can be operated in various wavelengths; after the exchange of the dyes, the alignment of the laser system is complex and the flexibility is expensive.



Source:[http://host.theeditors.com/laserscience/images/duo2202\\_big.gif](http://host.theeditors.com/laserscience/images/duo2202_big.gif)

Fig. 1-2 The wavelength coverage achieved with different classes of laser dye molecules



## Solid State Laser

Solid state lasers are becoming the laser of choice for many diverse applications. Selection of solid state lasers is based on their performance capabilities, such as available wavelengths, efficiency, tuning range, reliability, and pulse format flexibility. In solid state laser, there are three methods to tune the wavelength of the solid state laser : (1) broadband wavelength control; (2) narrow band wavelength control; (3) injection wavelength control. Broad wavelength control devices include prisms, gratings, and birefringent filters. For narrow tuning, a narrow wavelength control device must primarily contain the etalons in addition to the broad wavelength control device. With injection control, a narrow spectral bandwidth source is injected into the resonator to control the wavelength. The following table is the tuning range of the broadband solid state laser.


Name	Material	Transition	Spectral Range( $\mu\text{m}$ )
Ti:Sapphire	Ti:Al <sub>2</sub> O <sub>3</sub>	<sup>2</sup> E <sup>2</sup> T <sub>2</sub>	0.66-0.99
Alexandrite	Cr:BeAl <sub>2</sub> O <sub>4</sub>	<sup>4</sup> T <sub>2</sub> <sup>4</sup> A <sub>2</sub>	0.70-0.82
Cr:LiSAF	Cr:LiSrAlF <sub>6</sub>	<sup>4</sup> T <sub>2</sub> <sup>4</sup> A <sub>2</sub>	0.78-1.01
Co:MgF <sub>2</sub>	Co:MgF <sub>2</sub>	<sup>4</sup> T <sub>2</sub> <sup>4</sup> T <sub>1</sub>	1.5-2.3
LiF, F <sub>2</sub> <sup>+</sup>	LiF, 77K	$\sigma_u$ $\sigma_g$	0.82-1.05
KCl:Tl <sup>0(I)</sup>	Tl:KCl, 77K	<sup>2</sup> P <sub>3/2</sub> <sup>2</sup> P <sub>1/2</sub>	14-1.6

Table 1-3 The tuning range and the transition level of the solid state laser

## **Free Electronic Laser**

The free-electron laser (FEL) uses a relativistic beam of electrons passing through an undulating magnetic field (a wiggler) to produce stimulated emission of electromagnetic radiation. The general characteristics of the FEL are: (1) almost perfect mode quality; (2) high peak power; (3) very short pulse; (4) low duty cycles; (5) easily to tune the wavelength; (6) harmonic lasing. The resonant wavelength of the FEL depends on the electron energy, the wiggler magnetic field, the harmonic number, or the wiggler wavelength. So, changing these parameters could tune wavelength.

## **OPA and OPO**



The difference of OPA and OPO is mainly that OPO has the cavity and OPA pass the nonlinear crystal one trip. But the nonlinear mechanism of the two parametric interactions is the same; in other words, they employ the optical parametric generation in the second-order nonlinear phenomena. Under satisfying the energy conservation and momentum conservation (called as phase matching condition), one strong pump and one weak seeding interact in the nonlinear crystal, and the weak seeding is amplified with the emission of the idler beam. Since there is different wavelength satisfying the phase matching condition after rotating the crystal angle, the wavelength of the OPA/OPO is tuned by rotating the nonlinear crystal. This is a simple technique to tune the wavelength and the optimization just tunes the spatial and temporal overlap. The detailed theory about OPA is illustrated in the Chapter II.

The following table is the characterizations of the various OPAs [1].

Type	Pump Source			Specifications of OPA				
Material	$\lambda_p$ ( $\mu\text{m}$ )	$E_p$ (mJ)	$\tau_p$ (ps)	Tuning range ( $\mu\text{m}$ )	$E_{\text{out}}$ ( $\mu\text{J}$ )	$\Delta\nu$ ( $\text{cm}^{-1}$ )	$\tau_{\text{out}}$ (ps)	$\eta_{\text{max}}$ (%)
BBO-I	0.355	3	15	0.42-2.6	<700	4-10	<10	30
LBO-I	0.355	2.3	15	0.42-2.3	<300	>10	—	—
	0.355	8	18	0.41-2.85	<900	7-20	14	28
KDP	0.355	1.35	35	0.45-1.6	<300	10	8.37	10
BBO	0.532	8	25	0.67-2.58	<520	>20	18	20
	0.532	5	25	0.63-2.6	<250	1-2	25	10
LBO	0.532	5	25	0.65-2.5	<450	4-10	18	24
KDP	0.532	—	30	—	—	40	—	50
KTP	0.532	12	32	0.64-4.0	<1500	26	—	20
LiNbO <sub>3</sub>	0.532	0.7	7	0.59-3.7	—	20	—	10
LiNbO <sub>3</sub>	1.064	1	6	1.4-4.0	<10	6.5	3.5	1
KTP	1.053	28	50	1.57-4.0	<1800	31	—	20
AgGaS <sub>2</sub>	1.064	10	20	1.2-10	<100	8	10	10
BBO-I	0.532	1	1.3	0.63-3.2		200	0.7	25
BBO-II	0.532	1	1.3	0.63-3.2		55	0.7	20
KDP-II	0.532	1	1.3	0.77-1.7		23-28	0.7	13
BBO	0.60	0.09	190fs	0.75-3.1		180	180 fs	25
LBO	0.60	0.09	190fs	0.85-2.1		200	180 fs	15
BBO-I	0.78- 0.84	0.5	100fs	1.2-2.5	<50		100 fs	>10

Table 1-4 The characterization of the various OPA

## 1.4 Motivation and Objective

The ultrafast laser can be used in many applications, such as (1) fast temporal resolution (precisely triggering, controlling and sampling); (2) optical coherent tomography; (3) frequency comb; (4) high field physics and so on. The tunable laser benefits the spectroscopy. The Type-II optical parametric amplifier especially is suitable source for the time-resolved spectroscopy due to its nearly same pulse width.

In our laboratory, we develop the cascaded SFG of NOPA to generate 385nm to 465nm, single-shot OPA FROG to diagnose the characterization of the unknown pulse and white light OPA to generate the broadband pulse. Additionally, we also construct a near-IR tunable laser.



## 1.5 Organization of this thesis

In this thesis, I first outline the basic theory of optical parametric amplifiers and the ultra-broadband optical parametric amplifiers. In the chapter III, I explain the construction of the collinear Type-II OPA and its performance. For the next chapter, I describe the progress in the ultra-broadband OPA (white light OPA), including the essential experiments to understand why it has extremely broad bandwidth. Finally, I present a summary and suggest possible directions of future work.

# Chapter II Theoretical Background

In this chapter, the theory and concepts about optical parametric amplification are described [9]. These are separated into the basic OPA and the broadband OPA. The basic OPA states the propagation of the pulses in the nonlinear medium and some important parameters. For the broadband OPA, I illustrate the theory (or concepts) used in this thesis to study why the bandwidth in such a geometry could be broadened.

## 2.1 Basic Theory of Optical Parametric Amplification

I explain the concepts of the OPA and the coupled equations which state the propagation of the pulses inside the nonlinear medium. Then, the basic theory of OPA is separated into two parts according to the duration of the pump beam: first is non-ultrashort pulses which mean the continuous wave (CW) and the pulses that do not induce dispersion enough. The other is ultrashort pulses; in other words, the effect of different group velocities in the coupled equations must be considered. Finally, I illustrate the properties of several important parameters

### 2.1.1 Introduction of Optical Parametric Amplification

OPA is a three-wave mixing process in which the pump beam, the seeding (signal) beam and the idler beam at frequencies  $\omega_3$ ,  $\omega_1$  and  $\omega_2$ , respectively, with  $\omega_3 = \omega_1 + \omega_2$ , propagate and interact in a nonlinear medium. At the same time, the momentum conservation must be satisfied; phase matching condition  $\vec{k}_3 = \vec{k}_1 + \vec{k}_2$ . The geometries of

OPA have the collinear and non-collinear geometries, seeing the Fig. 2-1. Due to the different geometry, the two geometries have the different applications and characterizations.

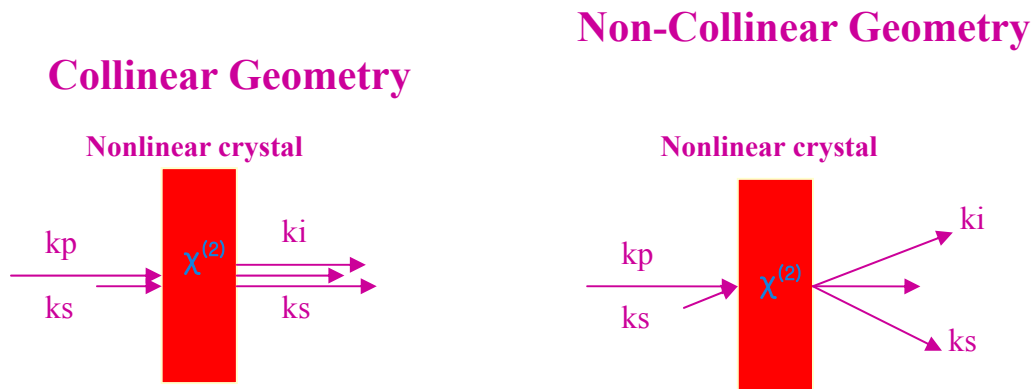


Fig.2-1 Geometries of OPA

Of the two geometries, the collinear OPA has wider tuning range because the tuning range of non-collinear OPA (NOPA) is limited by its angle between the pump beam and the signal. But NOPA has the possible of the broader band; this part is explained in the next section. OPA can also be classified according to the polarization of the three interacted beams. OPA can be divided into two regimes, Type-I and Type-II. In Type-I OPA, the polarizations of the pump beam, the signal and the idler are extra-ordinary (e) ray, ordinary (o) ray and o-ray respectively. The difference of two types is that the polarization of the idler beam in Type-II regime is e-ray. Besides, there is another type (called by Type-III) that exchanges the polarization of the signal and the idler of Type-II regime.

For simplicity, we will present theory of collinear OPA. The three waves propagating along z-axis under the collinear geometry are coupled through the second-order nonlinear polarization  $\vec{P}_{NL}(r,t)$  and are

governed by the wave equation:

$$\nabla \times \nabla \times \vec{E}(r,t) + \frac{1}{c^2} \frac{\partial^2}{\partial t^2} \vec{D}(r,t) = -\frac{4\pi}{c^2} \frac{\partial^2}{\partial t^2} \vec{P}_{NL}(r,t) \quad (2.1)$$

$\vec{E}(r,t)$  and  $\vec{D}(r,t)$  are the total electric field and displacement current given by

$$\vec{E}(r,t) = \sum_{n=1}^3 [\hat{e}_n \vec{A}_n(r,t) e^{i(\vec{k}_n \cdot \vec{r} - \omega_n t)} + c.c.] \quad (2.2)$$

$$\vec{D}(r,t) = \vec{E}(r,t) + 4\pi \vec{P}_L(r,t)$$

where  $\vec{A}_n$  is the complex slowly varying amplitude of the electric field of the n-th wave. The linear and nonlinear polarizations are related to the field by the constitutive relations:

$$\begin{aligned} \vec{P}_L(r,t) &= \int_{-\infty}^{\infty} \vec{\chi}^{(1)}(t-t') \cdot \vec{E}(r,t') dt' \\ \vec{P}_{NL}(r,t) &= \int_{-\infty}^{\infty} \int_{-\infty}^{\infty} \vec{\chi}^{(2)}(r,t-t_1, t-t_2) : \vec{E}(r,t_1) \vec{E}(r,t_2) dt_1 dt_2 \end{aligned} \quad (2.3)$$

which are valid in the electric-dipole approximation.

### 2.1.2 Coupled-wave equation

If the three waves are pulsed and quasi-monochromatic,  $\vec{\chi}^{(1)}(t-t')$  can be expanded into a Taylor series of  $(t-t')$  reflect the group-velocity mismatch and pulse spreading caused by material dispersion. And if the second-order response is assumed to be instantaneous and the pulse duration must be larger than 10fs, the nonlinear polarization can be written as the following form.

$$\begin{cases} P_{NL}(\omega_1) = \chi_{eff}^{(2)} A_3 A_2^* e^{i(\vec{k}_3 - \vec{k}_2) \cdot \vec{r} - i\omega_1 t} \\ P_{NL}(\omega_2) = \chi_{eff}^{(2)} A_3 A_1^* e^{i(\vec{k}_3 - \vec{k}_1) \cdot \vec{r} - i\omega_2 t} \\ P_{NL}(\omega_3) = \chi_{eff}^{(2)} A_1 A_2^* e^{i(\vec{k}_1 - \vec{k}_2) \cdot \vec{r} - i\omega_3 t} \end{cases}$$

where  $\chi_{eff}^{(2)}$  is the effective nonlinearity which depends on the beam polarization and the symmetry property of the second order tensor,  $\vec{\chi}^{(2)}$ .

Within the slowly varying amplitude approximation (SVA),  $(d^2 A / dz^2) \ll 2k(dA / dz)$ , the differential equation of the electric field can be simplified and decomposed into three coupled-wave equations.

$$\begin{cases} \hat{D}_1 A_1 = i \left( \frac{2\pi\omega_1}{cn_1} \right) \chi_{eff}^{(2)} A_3 A_2^* e^{i\Delta kz} \\ \hat{D}_2 A_2 = i \left( \frac{2\pi\omega_2}{cn_2} \right) \chi_{eff}^{(2)} A_3 A_1^* e^{i\Delta kz} \\ \hat{D}_3 A_3 = i \left( \frac{2\pi\omega_3}{cn_3} \right) \chi_{eff}^{(2)} A_1 A_2^* e^{-i\Delta kz} \end{cases} \quad (2.4)$$

where  $\Delta k = k_3 - k_1 - k_2$  is the phase mismatch and the differential operator  $\hat{D}_n$  is defined by

$$\hat{D}_n = \frac{\partial}{\partial z} + \rho_n \frac{\partial}{\partial x} + \frac{i}{2k_n} \left( \frac{\partial^2}{\partial x^2} + \frac{\partial^2}{\partial y^2} \right) + \frac{1}{v_{gn}} \frac{\partial}{\partial t} + i g_n \frac{\partial^2}{\partial t^2} \quad (2.5)$$

where

$$\left\{ \begin{array}{l} \rho_n, \text{ walk-off angle} \\ v_{gn}, \text{ group velocity, } v_{gn} = c/n_{gn} \text{ where } n_{gn} = n_n + \omega_n \left. \frac{\partial n_n}{\partial \omega} \right|_{\omega_n} \\ g_n, \text{ dispersion-spreading coefficient, } g_n = \left. \frac{1}{2} \frac{\partial^2 k}{\partial \omega^2} \right|_{\omega_n} \end{array} \right.$$



Since the coupled equations do not have the exact solution, it must be solved by numeric simulation. In order to understand its behavior inside the nonlinear medium, we take some approximations to the equation. But the approximations are valid under some limits. The next section introduces several lengths which may limit the length of the nonlinear crystal. By restricting the length of the crystal, we can simplify the coupled equation to comprehend the evolution of the behavior of the pulse.

### 2.1.3 Effective lengths [1]

(1) Aperture length ( $L_{an} = d_0 / \rho_n$ )

$d_0$  is beam diameter of a beam and  $\rho_n$  is the walk-off angle between the signal (or idler) and pump beams. It means the propagation distance that the e-ray is transversely displaced by  $d_0$ .

(2) Quasi-static interaction length ( $L_{qs} = \frac{\tau}{1/v_1 - 1/v_2}$ )

$\tau$  is pulse width.  $v_1$  and  $v_2$  are the group velocities of two pulses. The distance is over which the two pulses experience a relative time delay  $\tau$ .

(3) Diffraction length ( $L_{dif} = kd_0^2$ )

The beam diameter increases by a factor of  $2^{1/2}$  due to diffraction.

(4) Dispersion-spreading length ( $L_{ds} = \tau^2 / g_n$ )

The length is that the pulse would take to double its pulse width because of dispersion.

$$(5) \text{ Nonlinear interaction length } (L_{nl} = \frac{cn}{2\pi\omega A_0 \chi_{eff}^{(2)}})$$

The length means that the thickness of the nonlinear medium has significant energy transfer among the coupled waves for infinite plane waves.

## 2.1.4 Optical Parametric Amplification for non-ultrashort pulses

**Case I:** A depletionless pump beam (for crystal length  $L_c < L_{nl}$ )

Under the small-signal amplification limit (i.e.,  $L_c < L_{nl}$ ), Eq.(2.4) can be simplified as

$$\begin{cases} \frac{\partial A_1}{\partial z} = i \frac{2\pi\omega_1}{n_1 c} \chi_{eff}^{(2)} A_2^* A_3 \exp[i\Delta kz] \\ \frac{\partial A_2}{\partial z} = i \frac{2\pi\omega_2}{n_2 c} \chi_{eff}^{(2)} A_1^* A_3 \exp[i\Delta kz] \\ \frac{\partial A_3}{\partial z} = i \frac{2\pi\omega_3}{n_3 c} \chi_{eff}^{(2)} A_1 A_2 \exp[-i\Delta kz] \end{cases} \quad (2.6)$$

Using the Manley-Rowe relationship (photon conservation,  $\frac{1}{\omega_1} \frac{dI_1}{dz} = \frac{1}{\omega_2} \frac{dI_2}{dz} = -\frac{1}{\omega_3} \frac{dI_3}{dz}$ ),  $I_3(0) = I_{30} \gg I_{10}$ , and  $I_{20} = 0$ , the

solution of Eq(2.6) can be derived as:

$$\begin{cases} I_1(L) = I_{10} \left[ 1 + \frac{\Gamma^2}{g^2} \sinh^2(gL) \right] \\ I_2(L) = I_{10} \frac{\omega_2}{\omega_1} \frac{\Gamma^2}{g^2} \sinh^2(gL) \\ I_3(L) = I_{30} \end{cases} \quad (2.7)$$

where  $g = \sqrt{\Gamma^2 - (\Delta k/2)^2}$ ,  $\Gamma^2 = \frac{8\pi^2}{\varepsilon_0 c} (FM)^2 I_{30}$ ,  $FM = \frac{\chi_{eff}^{(2)}}{\sqrt{\lambda_1 \lambda_2 n_1 n_2 n_3}}$

### Case II: OPA with Pump depletion

If  $L_c > L_{nl}$ , strong energy exchange takes place in such a process. The signal and the idler are extremely amplified and the pump beam depleted in such process. Consider the interaction under the phase matching ( $\Delta k = 0$ ), the solution of Eq(2.6) can be expressed in terms of the Jacobian elliptic function, denoted as sn.

$$\begin{cases} I_1(L) = I_{10} + \frac{\omega_1}{\omega_3} I_{30} \left\{ 1 - sn^2 \left[ N\Gamma L - \frac{K(N)}{N^{1/2}}, N \right] \right\} \\ I_2(L) = \frac{\omega_2}{\omega_3} I_{30} \left\{ 1 - sn^2 \left[ N\Gamma L - \frac{K(N)}{N^{1/2}}, N \right] \right\} \\ I_3(L) = I_{30} sn^2 \left[ N\Gamma L - \frac{K(N)}{N^{1/2}}, N \right] \end{cases} \quad (2.8)$$

where

$$\begin{cases} K(N) = \frac{1}{4} \int_{-\pi}^{\pi} \frac{d\theta}{\sqrt{1 - N^2 \sin^2(\theta)}}, \text{ the complete elliptical function of the first kind} \\ N = \frac{1}{1 + (\omega_3 I_{10}) / (\omega_1 I_{30})}, \text{ the ratio of the number of photons in the input pump} \\ \text{beam to the total input photon number} \end{cases}$$

### 2.1.5 Optical Parametric Amplification Process for ultrashort pulses

Since the three ultrashort pulses have different group velocities in the nonlinear medium, the dispersive term must be added to the Eq(2.6). By using the pump moving with the group velocity ( $v_{gp}$ ) as the reference frame, the coupled equations are

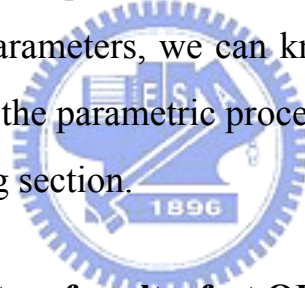
$$\begin{cases} \frac{\partial A_1}{\partial z} + \delta_{13} \frac{\partial A_1}{\partial \tau} = i \frac{2\pi\omega_1}{n_1 c} \chi_{eff}^{(2)} A_2^* A_3 \exp[i\Delta kz] \\ \frac{\partial A_2}{\partial z} + \delta_{23} \frac{\partial A_2}{\partial \tau} = i \frac{2\pi\omega_2}{n_2 c} \chi_{eff}^{(2)} A_1^* A_3 \exp[i\Delta kz] \\ \frac{\partial A_3}{\partial z} = i \frac{2\pi\omega_3}{n_3 c} \chi_{eff}^{(2)} A_1 A_2 \exp[-i\Delta kz] \end{cases} \quad (2.9)$$

where  $\delta_{13} = \left(\frac{1}{v_{g1}} - \frac{1}{v_{g3}}\right)$  and  $\delta_{23} = \left(\frac{1}{v_{g2}} - \frac{1}{v_{g3}}\right)$  are group velocities

mismatch (GVM) between the signal/idler and the pump beam.

Additionally,  $\delta_{12} = \left(\frac{1}{v_{g1}} - \frac{1}{v_{g2}}\right)$  is the GVM of the signal and the idler.

In general, the coupled equations do not have the exact solution. But, from several important parameters, we can know some characterizations of the amplified pulses in the parametric process. So, these parameters are illustrated in the following section.



### 2.1.6 Important parameters for ultrafast OPA

Except the above effective lengths, there are several important parameters including gain, phase matching angle, group velocity mismatch and bandwidth which are important for predicting the performance of the OPA.

#### (1) Gain

To understand the gain in the parametric process, we simplify the actual condition; so, we apply the Eq(2.7) to get the gain of the signal. Under the phase matching ( $\Delta k = 0$ ) and the large gain approximation ( $\Gamma L \gg 1$ ), the Eq(2.7) can be simplified as:

$$\begin{cases} I_1(L) \cong \frac{1}{4} I_{10} \exp(2\Gamma L) \\ I_2(L) \cong \frac{\omega_2}{4\omega_1} I_{10} \exp(2\Gamma L) \end{cases} \quad (2.10)$$

So, the gain of the signal is

$$G = \frac{I_1(L)}{I_{10}} = \frac{1}{4} \exp(2\Gamma L) \quad (2.11)$$

In 3mm-thickness BBO OPA pumped by 70GW/cm<sup>2</sup> and central wavelength of 800nm, the gain is about 10<sup>6</sup> at the signal of 1200nm.

## (2) Phase Matching Angle

For the collinear geometric structure, the phase matching condition is  $n_1\omega_1 = n_2\omega_2 + n_3\omega_3$ .

**For Type-I:**  $e(\text{pump}) \rightarrow o(\text{signal}) + o(\text{idler})$

$$n_{e3}(\theta_m)\omega_3 = n_{o2}\omega_2 + n_{o1}\omega_1 \quad (2.12)$$

And using the dependence of the extraordinary index on the propagation direction in uniaxial crystals

$$\frac{1}{n_{e3}^2(\theta_m)} = \frac{\text{Sin}^2(\theta_m)}{n_{e3}^2} + \frac{\text{Cos}^2(\theta_m)}{n_{o3}^2} \quad (2.13)$$

We can derive the phase matching angle

$$\theta_m = \text{ArcSin}\left[\frac{n_{e3}}{n_{e3}(\theta_m)} \sqrt{\frac{n_{o3}^2 - n_{e3}^2(\theta_m)}{n_{o3}^2 - n_{e3}^2}}\right] \quad (2.14)$$

**For Type-II:**  $e(\text{pump}) \rightarrow o(\text{signal}) + e(\text{idler})$

$$n_{e3}(\theta_m)\omega_3 = n_{o1}\omega_1 + n_{e2}(\theta_m)\omega_2 \quad (2.15)$$

Using Eq(2.13) and Eq(2.15), we can get the phase matching angle  $\theta_m$ .

For example, consider the BBO crystal (negative uniaxial crystal  $n_e < n_o$ ). The Sellmeier equation of the BBO crystal is

$$\begin{cases} n_o(\lambda) = [2.7359 + \frac{0.01878}{\lambda^2 - 0.01882} - 0.01354\lambda^2]^{1/2} \\ n_e(\lambda) = [2.7359 + \frac{0.01224}{\lambda^2 - 0.01667} - 0.01516\lambda^2]^{1/2} \end{cases}$$

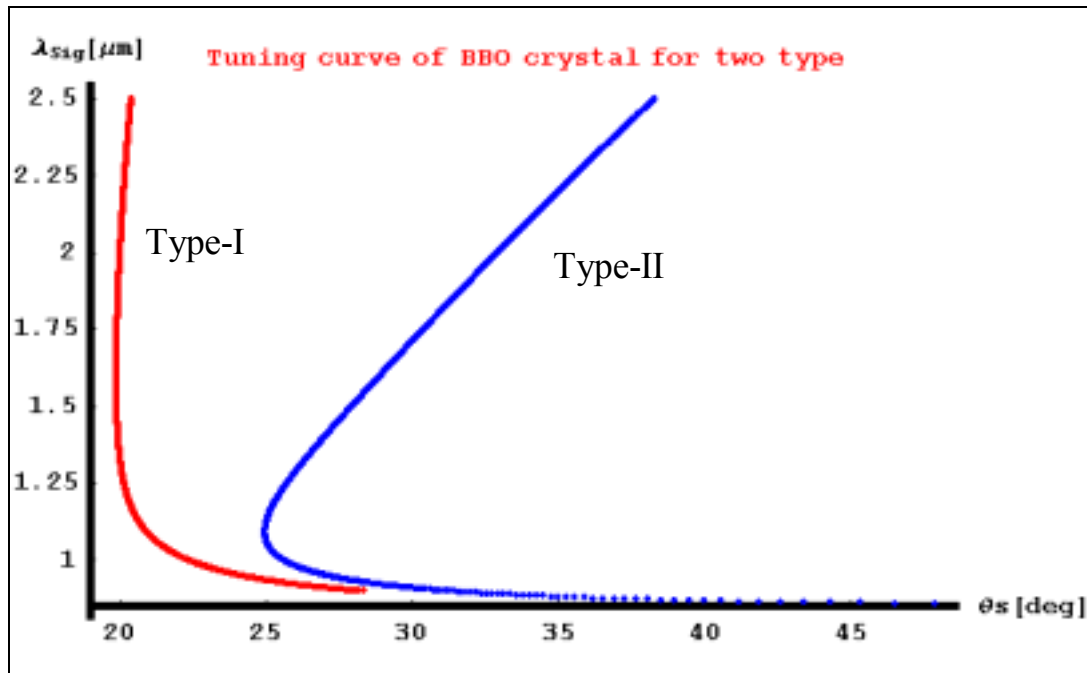


Fig.2-2 Phase Matching Curve of OPA pumped by  $\lambda_3 = 0.8\mu m$

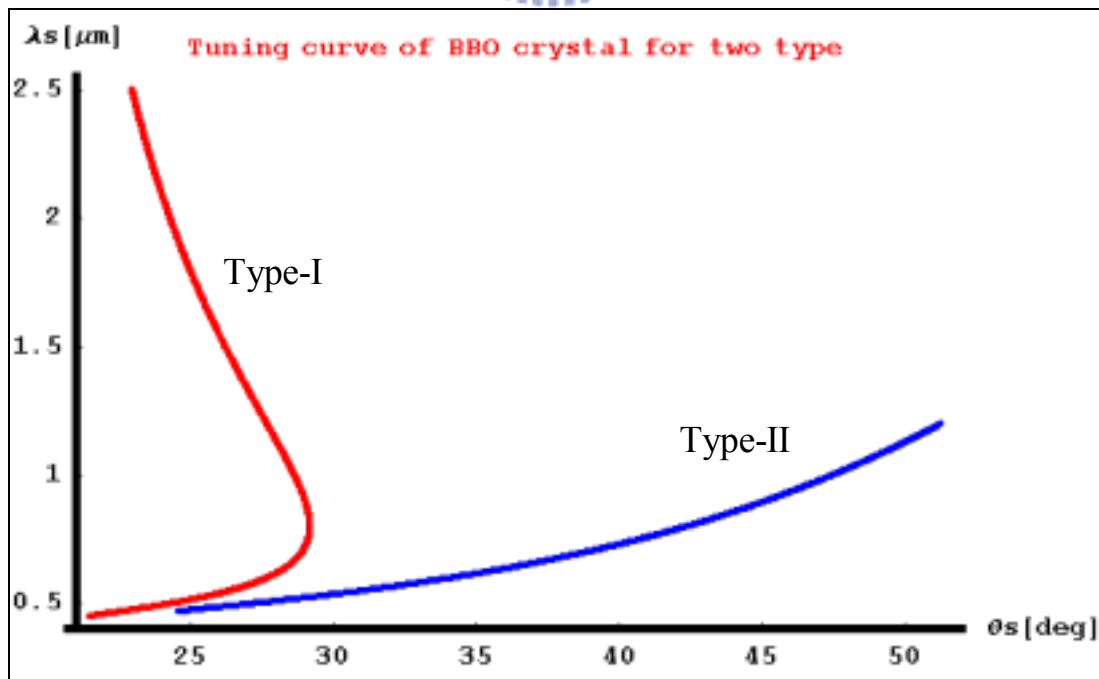
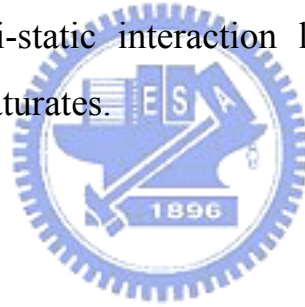


Fig.2-3 Phase Matching Curve of OPA pumped by  $\lambda_3 = 0.4\mu m$

### (3) Group Velocity Mismatch (GVM) for $\delta_{13}$ and $\delta_{23}$

#### **Case I :** $\delta_{13}\delta_{23} > 0$

Both the signal and the idler are away from the pump beam in the same direction, so the parametric interaction of the signal/idler and the pump beam disappear for the propagation distance longer than the quasi-static interaction length. Since the OPA pumped by  $\lambda_3 = 0.4\mu m$  and the Type-I OPA pumped by  $\lambda_3 = 0.8\mu m$  belong to this condition shown in the Fig.2-4 and Fig.2-5, the crystal length under this situation is limited by the GVM. The phenomena can be proven by numerical solving the differential equation [9]. Its solution show that when the crystal length is longer than the quasi-static interaction length, the signal can not increase and eventually saturates.



#### **Case II :** $\delta_{13}\delta_{23} < 0$

In this case, the signal and the idler move in the opposite direction with respect to the pump beam, seeing the Type-II of Fig. 2-4. It seems that the two pulses stay localized under the pump pulse, so the gain continuously increases as the crystal length increases. Its thought is that the signal slightly moves to the left of the pump; in the parametric process, the signal generates the idler and the idler moves to the right through the peak of the pump beam. Then, the idler also generates the signal, and the signal moves to the left toward the peak of the pump beam. So, in this regime, increasing the crystal length is also increasing the gain of the signal. The solution of such coupled equations proves that the gain is not limited by the crystal length [9].

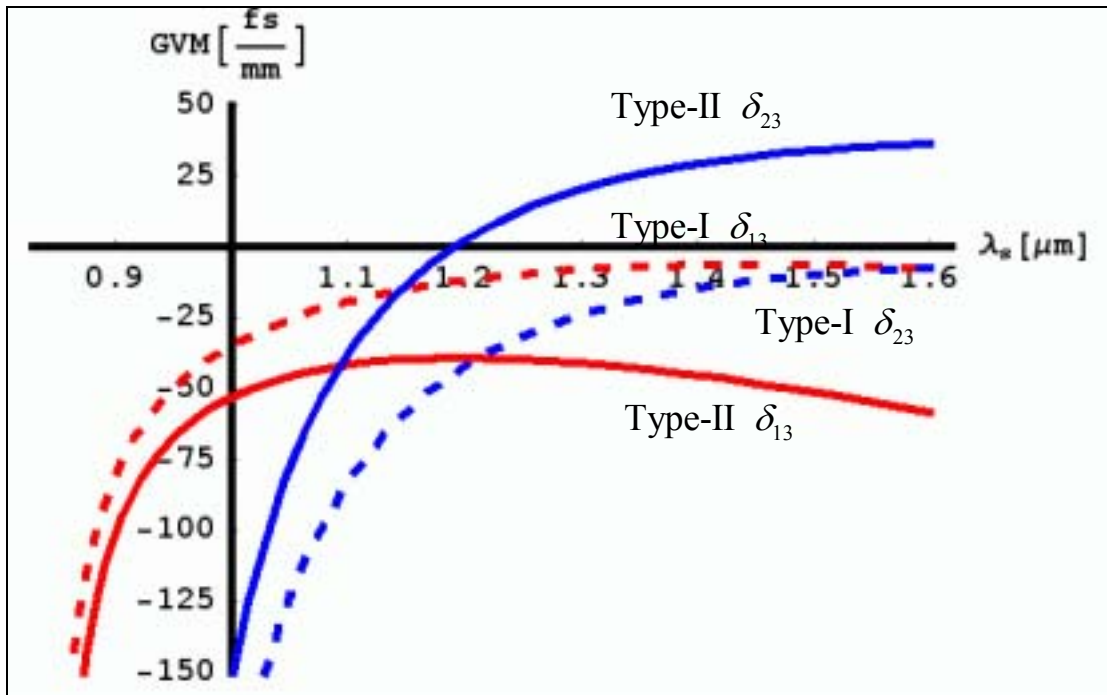


Fig.2-4 Group Velocity Mismatch of BBO pumped by  $\lambda_3 = 0.8 \mu\text{m}$

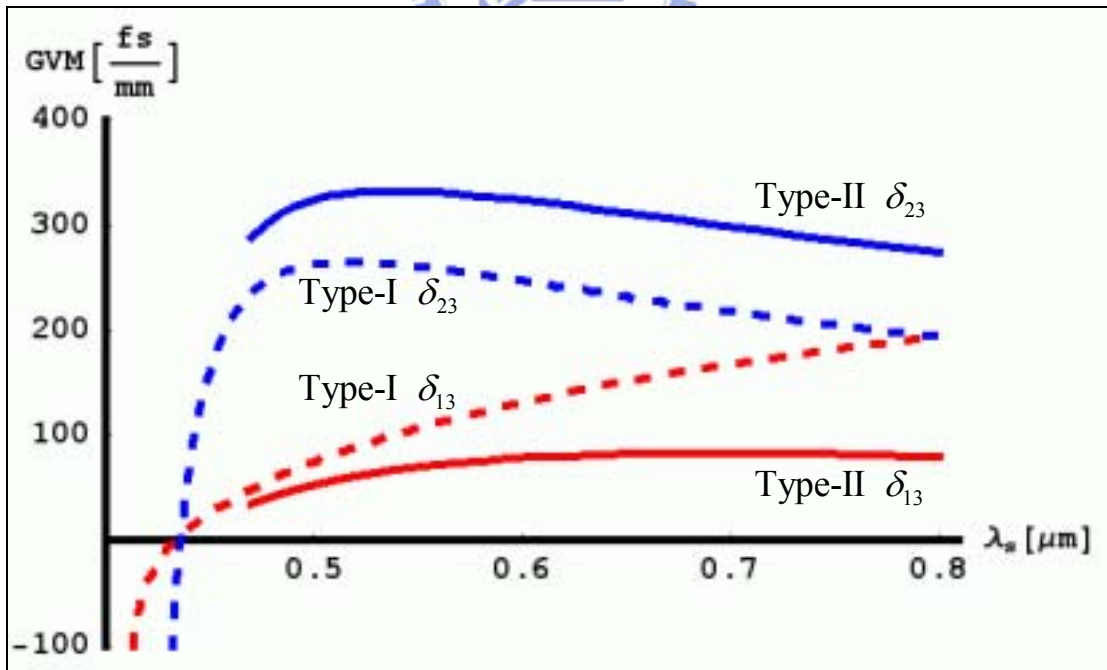


Fig.2-5 Group Velocity Mismatch of BBO pumped by  $\lambda_3 = 0.4 \mu\text{m}$



#### (4) Bandwidth

The phase matching bandwidth for the parametric amplification process is determined by the group velocity mismatch of the signal and the idler. If the frequency of the signal slightly increases, the induced wave vector mismatch ( $\Delta k$ ) is approximated to the first order as:

$$\begin{aligned}\Delta k &\cong k_3 - \frac{n_1(\omega_1 + \Delta\omega)}{c_0} - \frac{n_2(\omega_2 - \Delta\omega)}{c_0} - \frac{\partial k_1}{\partial \omega_1} \Delta\omega + \frac{\partial k_2}{\partial \omega_2} \Delta\omega \\ &= \left( \frac{n_2 - n_1}{c_0} \right) \Delta\omega + \left( \frac{1}{v_{g2}} - \frac{1}{v_{g1}} \right) \Delta\omega = \left( \frac{n_2 - n_1}{c_0} + \delta_{21} \right) \Delta\omega\end{aligned}\quad (2.16)$$

To calculate the full width at half maximum (FWHM) of the intensity of the signal within large-gain approximation, we can get the acceptable wave vector mismatch. And then the bandwidth is

$$\Delta\nu \cong \frac{2\sqrt{\ln 2}}{\pi} \left( \frac{\Gamma}{L} \right)^{\frac{1}{2}} \frac{1}{\frac{n_2 - n_1}{c_0} + \delta_{21}} \quad (2.17)$$

The broader bandwidth can be completed within group velocity match under some special condition, such as degeneracy in Type-I OPA ( $\delta_{21} = 0$ ). The bandwidth of BBO OPA is shown in the Fig. 2-6 and Fig. 2-7. From these simulations, Type-I OPA has the broader bandwidth because the signal and the idler have the same polarizations resulting in the smaller group velocity mismatch. Type-II OPA has nearly the bandwidth over the all tuning range. These feature can be exploited for different applications: Type-I phase matching is used to achieve the shortest pulses, while Type-II phase matching allows to obtain relatively narrow bandwidths over broad tuning ranges, which are required for many spectroscopic investigations.

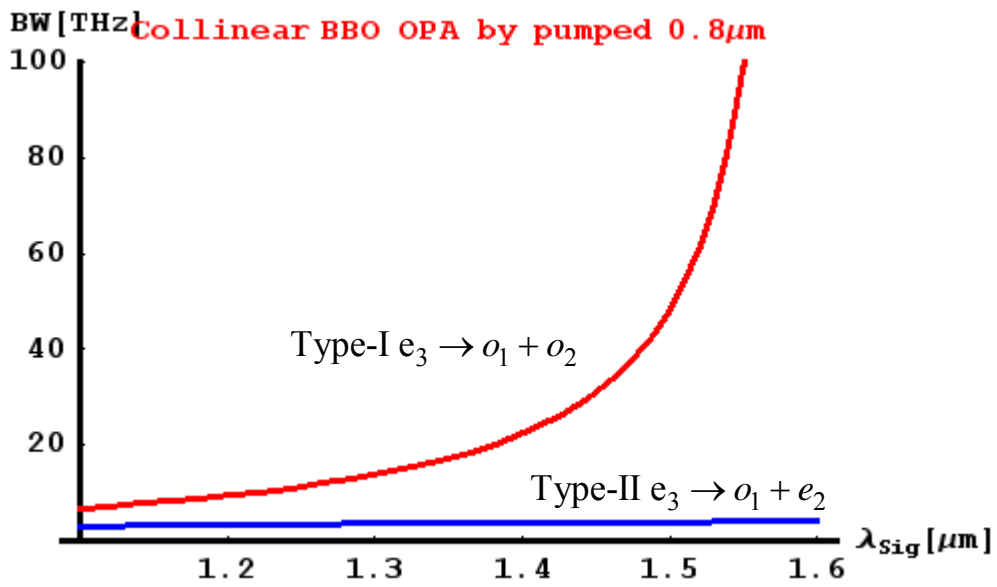


Fig.2-6 Phase Matching Bandwidth of BBO OPA pumped by  $\lambda_3 = 0.8\mu\text{m}$

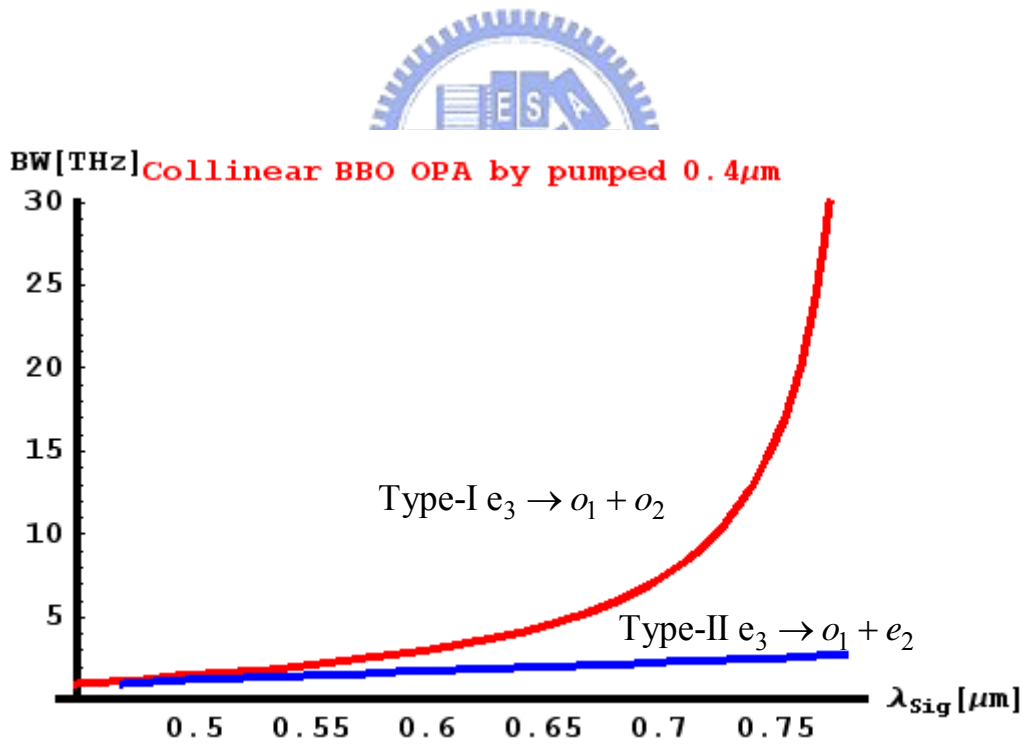


Fig.2-7 Phase Matching Bandwidth of BBO OPA pumped by  $\lambda_3 = 0.4\mu\text{m}$

## 2.2 Theory of ultra-broadband source generation

In this section, I describe the theory and concept of the ultrabroadband pulse including the NOPA, two-beam pump OPA and single-shot geometric scheme in order.

### 2.2.1 Non-collinear Optical Parametric Amplification [9]

The geometry of NOPA is shown Fig. 2-8(a). The angle  $\alpha$  is between the pump and the signal. The other angle  $\Omega$  is between the idler and the signal.

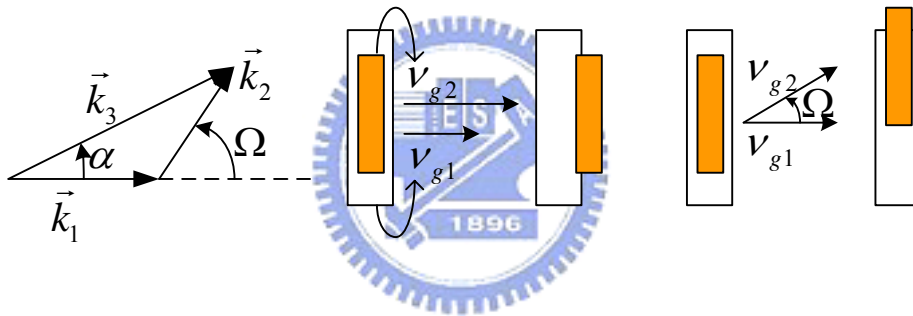


Fig. 2-8 (a) the geometry of NOPA; (b) the propagation situation of the signal and the idler for the collinear interaction; (c) same as (b) for the noncollinear interaction

From the Fig. 2-8(b), we know that in the collinear interaction, the signal (white block) and the idler (yellow block) separate after the quasi-static interaction length. But for the noncollinear interaction seeing Fig. 2-8(c), they separate along the transverse direction and stay effectively overlapped for the longitudinal direction. So, it is possible to accomplish the smaller GVM for NOPA by suitable angle between the pump and the signal. In the noncollinear geometry, the phase matching condition must be separated into two directions (parallel or perpendicular

to the signal). It can be written as Eq(2.19).

$$\begin{cases} \Delta k_{\parallel} = |\vec{k}_3| \cos \alpha - |\vec{k}_1| - |\vec{k}_2| \cos \Omega \\ \Delta k_{\perp} = |\vec{k}_3| \sin \alpha - |\vec{k}_2| \sin \Omega \end{cases} \quad (2.19)$$

where  $\Omega$  depends on the wavelength of the signal.

Take the first order approximation of the wave vector mismatch as

$$\Delta k_{\parallel} \cong \left( \frac{n_2 \cos \Omega - n_1}{c_o} - \frac{\partial k_1}{\partial \omega_1} + \frac{\partial k_2}{\partial \omega_2} \cos \Omega - k_2 \sin \Omega \frac{\partial \Omega}{\partial \omega_2} \right) \Delta \omega \quad (2.20)$$

$$\Delta k_{\perp} \cong \left( \frac{n_2 \sin \Omega}{c_o} + \frac{\partial k_2}{\partial \omega_2} \sin \Omega + k_2 \cos \Omega \frac{\partial \Omega}{\partial \omega_2} \right) \Delta \omega \quad (2.21)$$

For the first order term,

$$\text{Eq(2.20)} \times \cos \Omega + \text{Eq(2.21)} \times \sin \Omega \Rightarrow \frac{\partial k_2}{\partial \omega_2} - \cos \Omega \frac{\partial k_1}{\partial \omega_1} = 0$$

$$\text{The condition is equivalent to } v_{g1} = v_{g2} \cos \Omega \quad (2.22)$$

The Eq(2.22) states the broadband condition. Only if  $v_{g2} > v_{g1}$ , the Eq(2.22) is satisfied. It always happens in the commonly used Type-I phase matching in the negative uniaxial crystals. Use the Eq(2.19) and Eq(2.22) to find the angle between the pump beam and the signal,  $\alpha$ .

$$\alpha = \arcsin \left( \frac{1 - v_{g1}^2 / v_{g2}^2}{1 + 2v_{g1}n_1\lambda_2 / v_{g2}n_2\lambda_1 + n_1^2\lambda_2^2 / n_2^2\lambda_1^2} \right)^{1/2} \quad (2.23)$$

Consider the Type-I BBO OPA pumped at  $\lambda_3 = 0.4 \mu m$ . The simulation of the phase matching curve of various  $\alpha$  is shown in Fig. 2-9. In most  $\alpha$ , one phase matching angel is corresponding to one wavelength, except for  $\alpha = 3.7^\circ$ . When  $\alpha = 3.7^\circ$  and phase matching angle is about 31 degree, there are various wavelengths satisfying the phase matching condition at the same time.

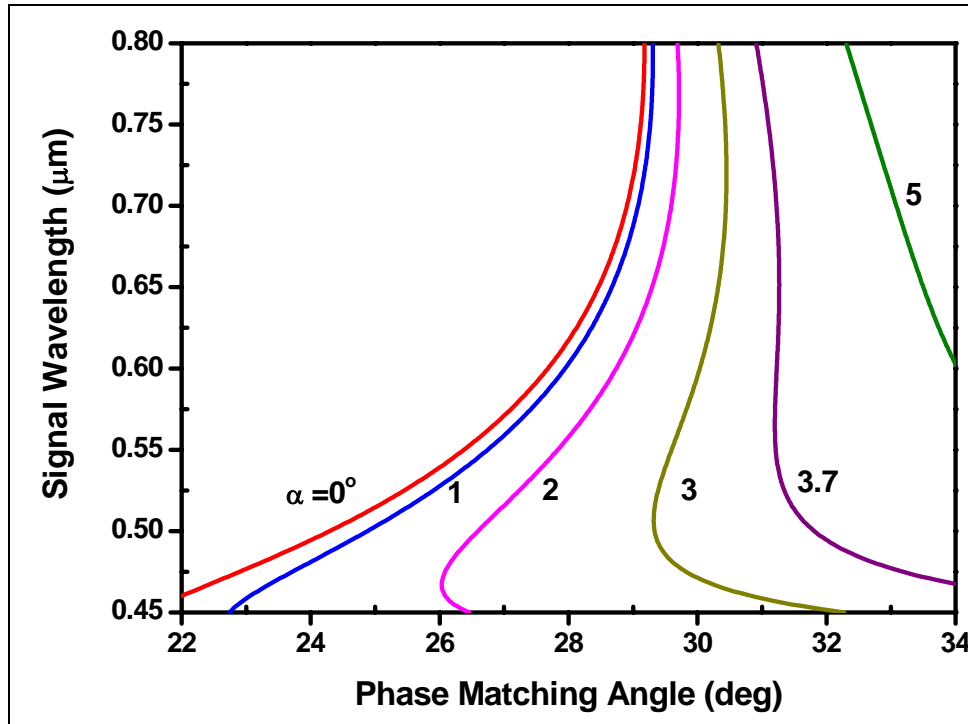


Fig. 2-9 Phase Matching curves of NOPA for various included angles

### 2.2.2 Two-beam pump (Multi-beam pump) OPA [5]

Its main concept is that two pump beams and the seeding beam interact in the nonlinear medium at various phase matching angles, so there are amplified signal with various central wavelengths and its individual bandwidth. If the central wavelengths of the two signals are closer enough but different, the effective bandwidth combines the individual bandwidth. Fig. 2-10(a) shows the geometry of the nonlinear crystal. The two pump beams lie on the  $\phi$  plane of the uniaxial crystal. The angles between the two pumps and the signal are  $\alpha_1$  and  $\alpha_2$  respectively. The  $\theta$  is between the signal and the optical axis. Fig. 2-10(b) is the phase matching curve for different  $\theta$  in such an OPA by pumped 400nm. The blue, red and green are for  $\theta = 28.20^\circ$ ,  $28.46^\circ$  and  $28.67^\circ$  respectively. In the Fig. 2-11(a), the spectrum (the solid line) has the broader band than the individual spectrum (the dash line). The

wavelength of the pump is 527nm and the  $\alpha$  of the two pump beams are  $0.78^\circ$  and  $0.60^\circ$  corresponding to 716nm and 727nm of the signal. The  $\theta$  is about  $21.75^\circ$  and its corresponding phase matching curve is shown in Fig. 2-11(b). From this result, we extend the concept to multi-beam pump by the cylindrical mirror. The beam is lengthened by a cylindrical mirror with a short focal length and hit the nonlinear crystal by another cylindrical mirror with a long focal length. The detail is described in the white light OPA.

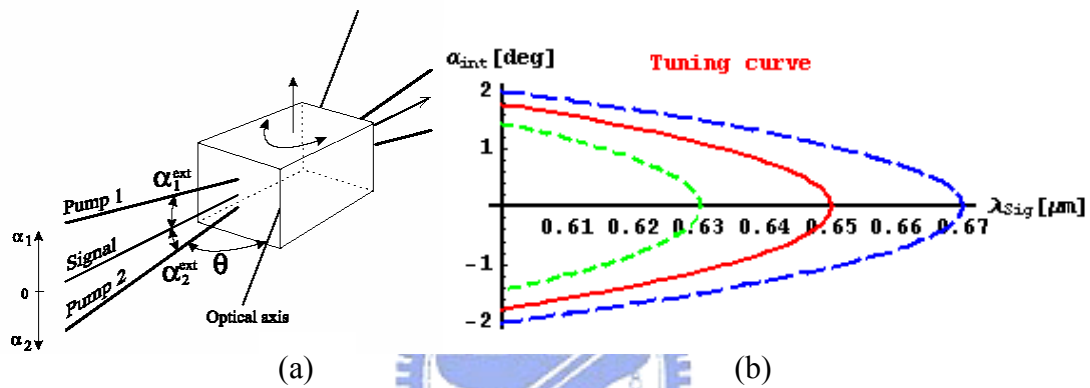


Fig. 2-10 (a) The geometry of the nonlinear crystal and the incident beams; (b) The Phase Matching Curve for the pump beam at various  $\theta$

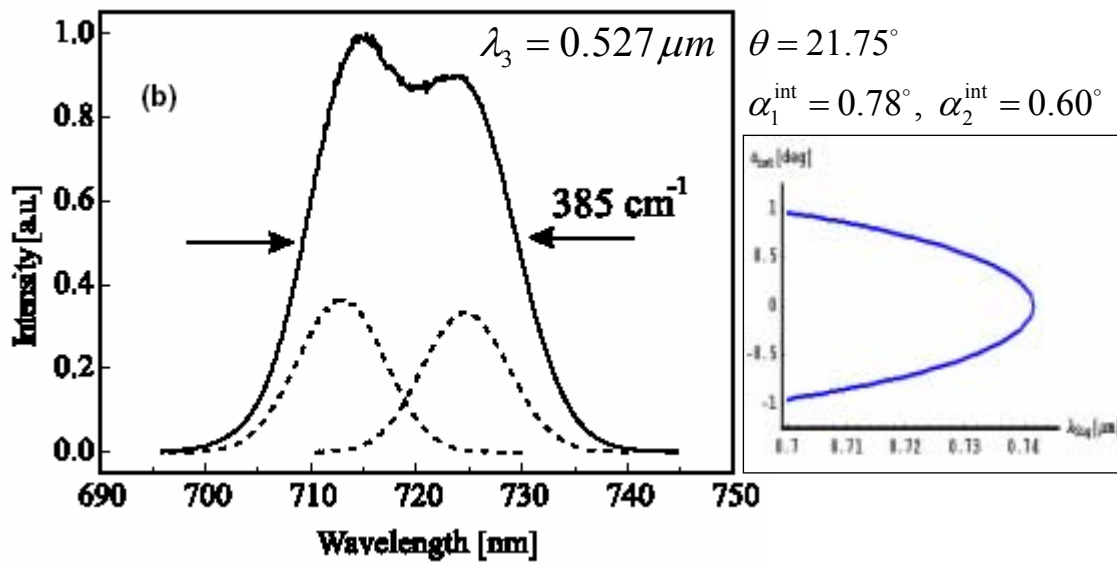


Fig. 2-11 Amplified Signal Spectral and phase-matching curve

### 2.2.3 Single shot geometric scheme [10]

The different wavelength of the amplified signal need the different delay of the pump and the signal in the multi-beam pump OPA described as the above section. In order to satisfy the condition, we utilize the single shot geometric scheme shown Fig. 2-12. The delay ( $\Delta\tau$ ) included in the induced signal due to two pulses interacted inside the nonlinear crystal contains various delays of the two pulses. The single shot geometric scheme can compensate the different delay for the different wavelength of the amplified signal.

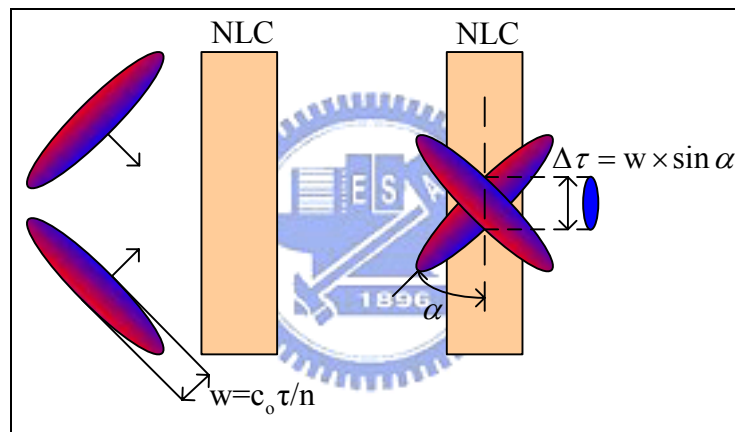


Fig. 2-12 Single shot geometric scheme

So, the cylindrical mirror replaces of the spherical mirror. Only one axis is focusing and the other axis can be used to complete the single shot geometric scheme.

## 2.2.4 White Light OPA

White light OPA combines the NOPA, the two-beam pump OPA and the single shot geometric scheme. NOPA can provide the broader bandwidth. From the two beam pump OPA, we use a pair of cylindrical mirror to lengthen the spot size, such as multi-beam pump. The multi-beam pump can amplify the different wavelength of the seeding beam. Using the single shot geometric structure increases the various delays to compensate the lack of the multi-beam pump. The following is to understand the phase matching curve under such condition.

### Geometry structure

The geometry of the white light OPA is shown in Fig. 2-13. For (a) the geometry of the k-space, the  $k_s$  is along the  $k_z$ -axis. Fig. 2-13(b) is the actual geometry of the nonlinear crystal. The signal and the optical axis have an angle,  $\theta$ . The signal and the pump have two angles,  $\alpha$  and  $\beta$  described in the Fig. 2-14. In the Fig. 2-14,  $\alpha$  is the angle between the pump and the signal projected onto the Y-Z plane and  $\beta$  is the angle between the pump and the signal projected onto the X-Z plane.

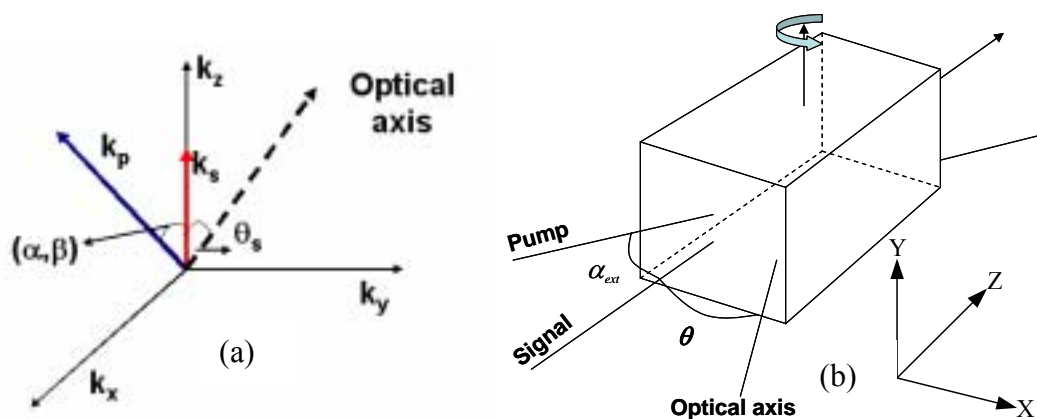


Fig. 2-13 (a) The geometry of the k-space; (b) The geometry of the nonlinear crystal



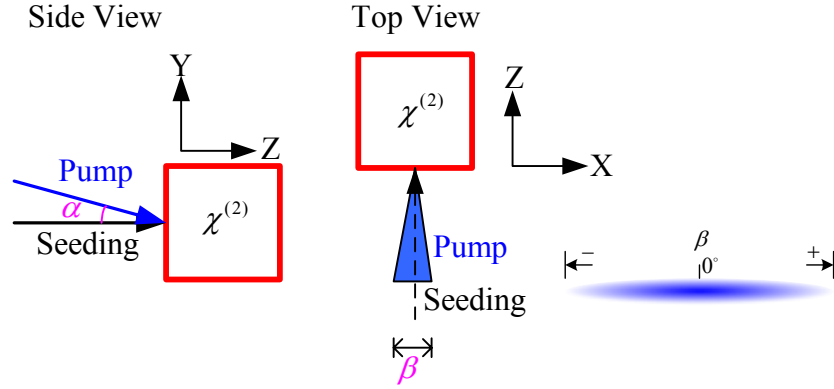


Fig. 2-14 The detail structure of the angles of the interacted pulses

### Phase matching condition under the above geometry

According to the diagram of the k-vector and the momentum conservation for the nonlinear crystal under Type-I OPA, we can calculate and simulate the phase matching curve of  $\beta$  v.s.  $\lambda_{sig}$ .

First, the momentum conservation

$$\vec{k}_3 = \vec{k}_1 + \vec{k}_2 \quad (2.24)$$

Second, from the diagram of the k-vector,  $\vec{k}_3$  and  $\vec{k}_2$  can be written as

$$\begin{cases} \vec{k}_3 = (k_3 \cos \beta \sin \alpha, k_3 \sin \beta, k_3 \cos \beta \cos \alpha) \\ \vec{k}_1 = (0, 0, k_1) \end{cases} \quad (2.25)$$

Additionally, the optical axis is  $(0, \sin \theta_1, \cos \theta_1) = \vec{o}$ .

Then  $\theta_3$  is known as:

$$\begin{aligned} \vec{k}_3 \cdot \vec{o} &= k_3 \cos \theta_3 = k_3 \sin \beta \cdot \sin \theta_1 + k_3 \cos \beta \cos \alpha \cdot \cos \theta_1 \\ \Rightarrow \theta_3 &= \arcsin \sqrt{1 - (\sin \beta \sin \theta_1 + \cos \beta \cos \alpha \cos \theta_1)^2} \end{aligned} \quad (2.26)$$

and the angle between the lengthened pump and the signal is

$$\alpha' = \arcsin \sqrt{1 - (\cos \alpha \cdot \cos \beta)^2} \quad (2.27)$$

Substitute Eq(2.27) into the equation  $|\vec{k}_2|^2 = |\vec{k}_3|^2 + |\vec{k}_1|^2 - 2\vec{k}_3 \cdot \vec{k}_1$ .

$$\begin{aligned}
\text{Then, } & \left( \frac{n_e^{(3)}(\lambda_3, \theta_3)}{\lambda_3} \right)^2 + \left( \frac{n_o^{(1)}(\lambda_1)}{\lambda_1} \right)^2 - \left( \frac{n_o^{(2)}(\lambda_2)}{\lambda_2} \right)^2 \\
& = 2 \frac{n_o^{(1)}(\lambda_1)}{\lambda_1} \cdot \frac{n_e^{(3)}(\lambda_3, \theta_3)}{\lambda_3} \cos \alpha \cos \beta
\end{aligned} \tag{2.28}$$

Substitute the Eq (2.26) into the Eq (2.28), and fix the two angles ( $\theta_1$  and  $\alpha$ ) to simulate the phase matching curve,  $\beta$  v.s.  $\lambda_{sig}$ .

### The Simulation Result

Consider the BBO crystal for Type-I OPA pumped by the SHG of a regeneratively amplified Ti:Sapphire laser (Spitfire, Spectra Physics) with a central wavelength of 800 nm, repetition rate of 1 KHz and pulse duration of ~50 fs.

Choose  $\alpha = 1^\circ$  and  $\theta_1 = 28.46^\circ$  (the angle corresponds to the wavelength of  $0.65\mu\text{m}$  satisfying the phase matching condition for collinear Type-I OPA).

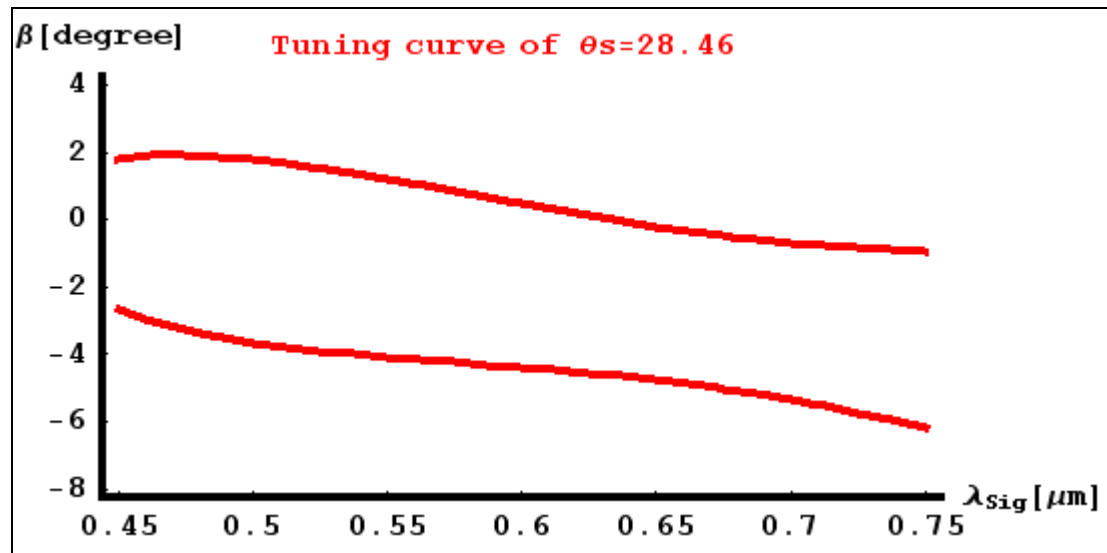


Fig.2-15 Phase Matching Angle of white light OPA with BBO crystal by pumped  $\lambda_3 = 0.4\mu\text{m}$

From the curve in Fig. 2-15, we can understand that if we attempt to generate the ultra-broad bandwidth source, only let the BBO crystal be pumped at the most angles of the above curve simultaneously. So, the pump beam is expanded into straight line and focusing on the crystal by the cylindrical mirror. Then the incident pump beam is viewed as multi-beam pump at various angles. So, the central wavelength of the phase matching signal contains quite large range and the amplified signal spectral has very broad bandwidth. The output by using suitable compressor to compensate the group velocity dispersion is the ultrafast laser with the duration of few-cycle. Since the lengthened pump is incident from the two side of the signal, the phase matching curve has two curves (positive and negative  $\beta$ ). Although the curve is not symmetry about  $\beta = 0$  due to the non-zero angle of the signal and the optical axis, we want to understand how  $\theta_s$  affects the phase matching curve. So, we simulate these curves at different  $\theta_s$  shown in Fig. 2-16.

In Fig. 2-16, there are some interesting phenomena. It does not have the symmetrical situation and tends to the negative angles with the same slope at different  $\theta_s$ . The breach of the phase matching pattern is toward the longer wavelength around  $0.7\mu\text{m}$ . Even, the phase matching curve forms a close-loop at some incident angles. It means that two wavelengths can satisfy the phase matching condition simultaneously. This also explains that the phase matching bandwidth is limited over some region. The break point about  $0.7\mu\text{m}$  is connected when  $\theta_s$  is larger than  $27.6^\circ$ . If we want to generate the broadband signal, the  $\theta_s$  must be larger than  $27.6^\circ$ . Or the wavelength of  $0.7\mu\text{m}$  may be not amplified.

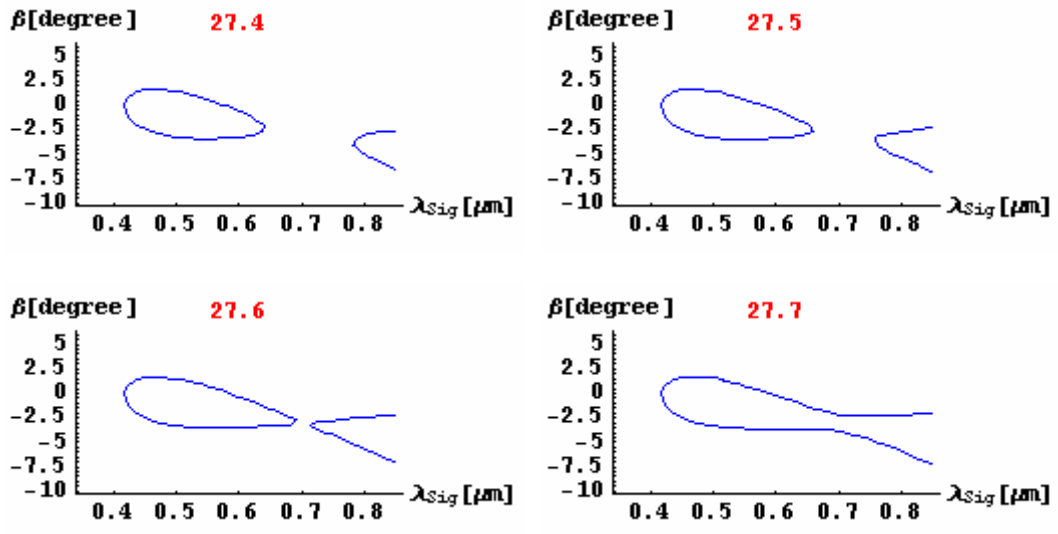


Fig. 2-16 The phase matching curves at different  $\theta_s$



# Chapter III Collinear Optical Parametric Amplifiers

## 3.1 Experimental system configuration

The configuration of the collinear optical parametric amplification system is shown in the Fig.3-1. The OPA was pumped by a regeneratively amplified Ti: Sapphire laser (Spitfire, Spectra Physics) with a central wavelength of 800 nm, repetition rate of 1 KHz and pulse duration of ~50 fs. The spectrum of the laser seeing the Fig. 3-2 has the full width half maximum of ~40nm. The measured result of the single shot autocorrelator seeing the Fig. 3-3 shows the pulse duration of ~50fs after the conversion of the unit. A small part of the Spitfire output was split from a beam splitter (5/95) to generate the white light continuum using a sapphire plate. The remaining pulse energy of the pump laser was further split using a (15/85) beam splitter to pump the two stage of the OPA. First stage of the OPA was collinearly pumped by 70 $\mu$ J from the Spitfire with white light seeding using the BBO (type II, z-cut at 27 $^{\circ}$ ) nonlinear crystal. The collimated output of the OPA was then passed through the same BBO crystal together with the remained pumping energy (~350 $\mu$ J) to accomplish the two-stage OPA. The Fig.3-4 is the actual system and the SHG of the signal.

We retrieve the amplitude and the phase of the generated OPA output using the frequency resolved of optical gating (FROG) at several wavelengths over all tuning range. The FROG system is shown as Fig. 3-5.

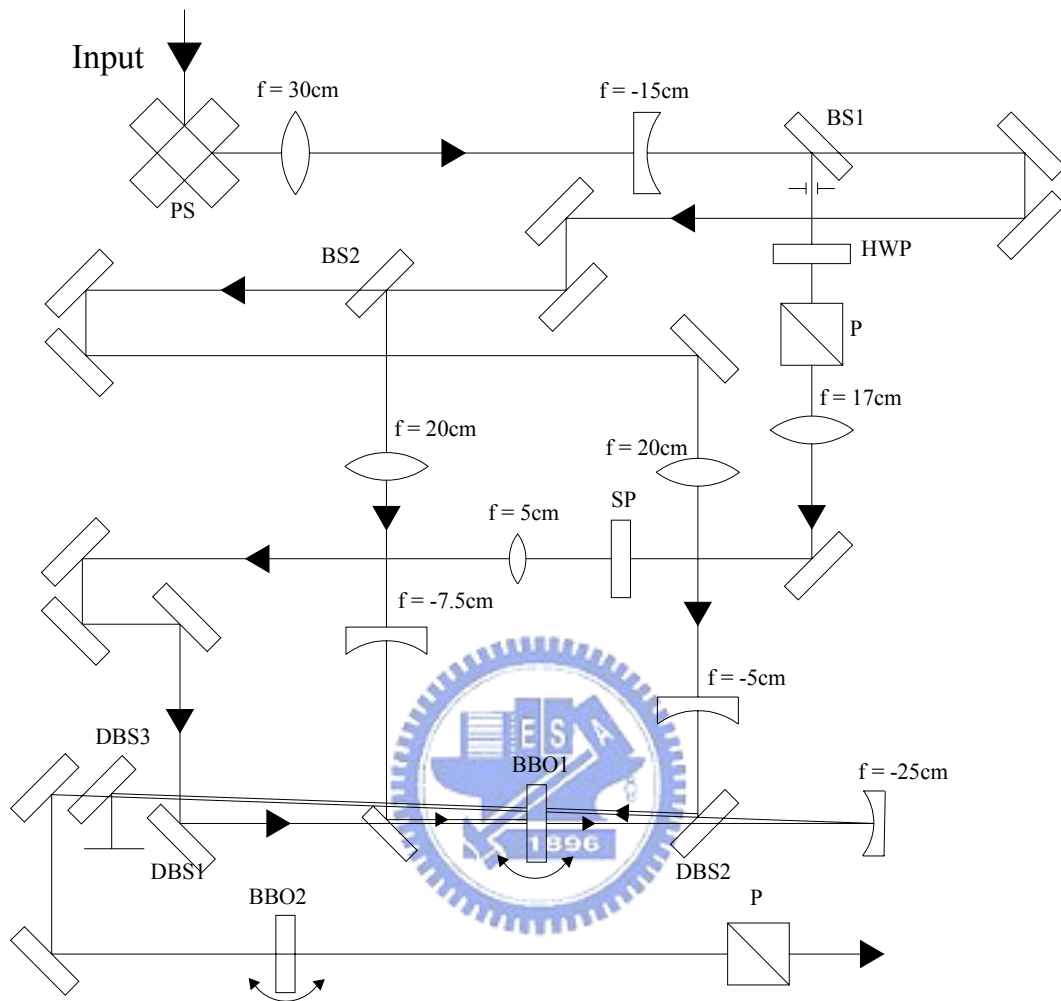


Fig. 3-1 The configuration of the collinear optical parametric amplification

PS: Periscope

BBO2: BBO for SHG

HWP: Half-wave plate

SP: Sapphire plate

BBO1: BBO for OPA

BS1,2:(5/95),(15/95) beam splitter

P: Polarizer

DBS1, 2, 3: Dichroic beam splitter

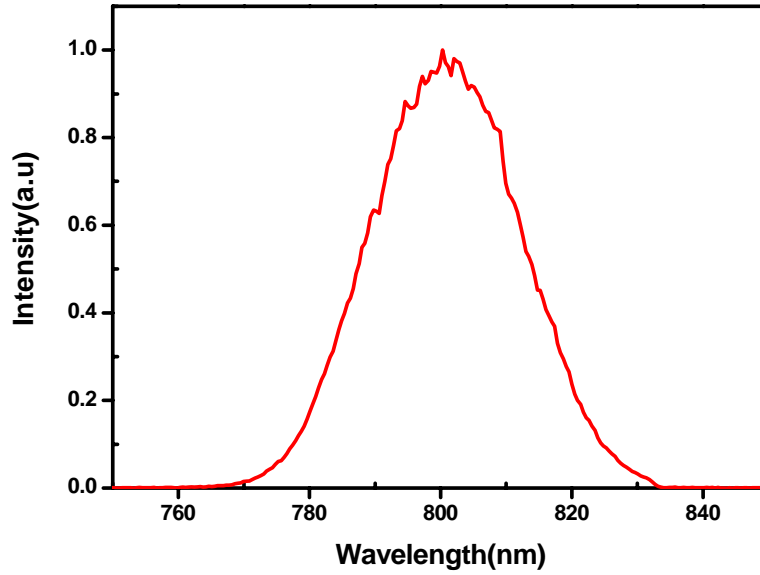


Fig. 3-2 Spectrum of SpitFire

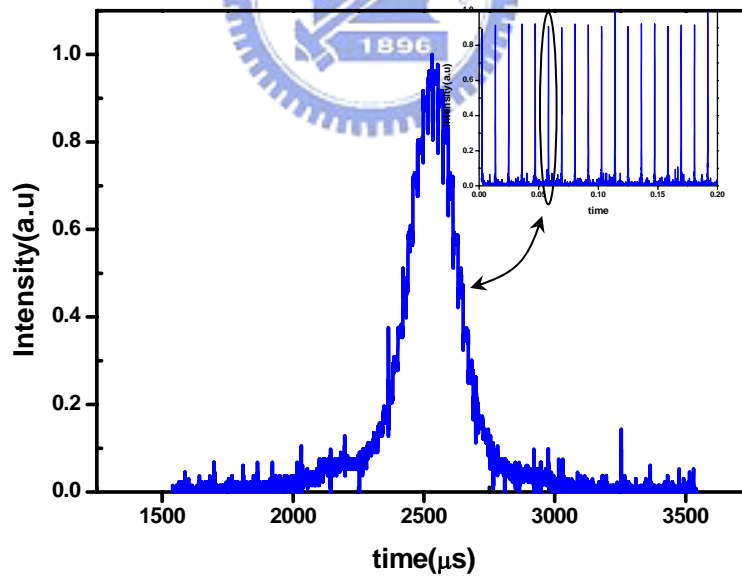


Fig. 3-3 The result of the single shot autocorrelator

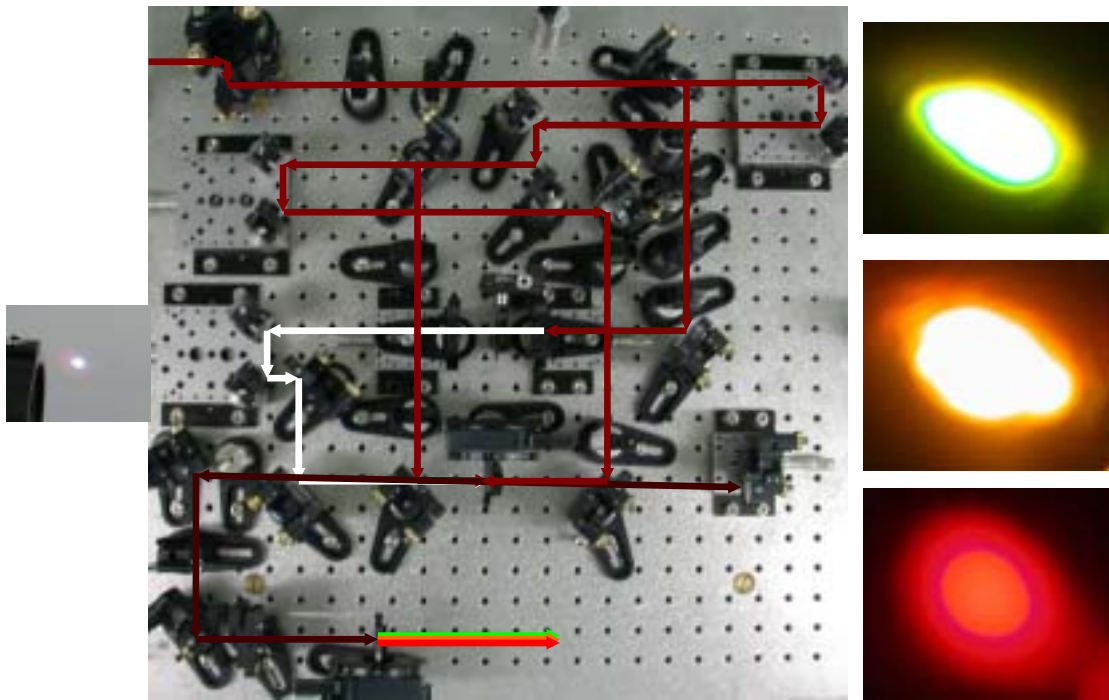


Fig. 3-4 The actual configuration and the SHG of the IR output

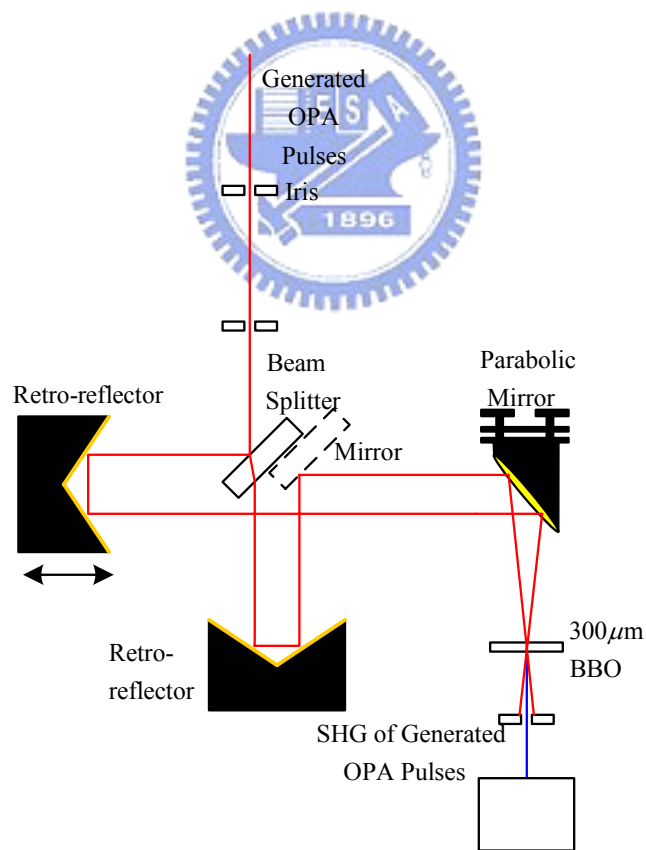


Fig. 3-5 The FROG System Setup



## 3.2 Result of Collinear Optical Parametric Amplifiers

The retrieved amplitude and phase of the collinear optical parametric amplifiers are shown from Fig. 3-6 to Fig. 3-10 at wavelength of 1141, 1227, 1294, 1447, and 1524nm, respectively. From the result, the durations of various wavelengths have nearly the pulse width of ~50fs as the same as the expected pulse width. The average power of various wavelengths is from ~20mW to ~50mW and the conversion efficiency is about 10%. These characterizations of the collinear OPA are summarized in the Table 3-1 including the phase matching angle, bandwidth, duration, and average power. Fig. 3-11 shows the individual spectrum of the different wavelength. We compare the measured tuning curve with the theoretical one, shown as Fig. 3-12. The error between both curves is smaller than 1 degree. So, the measured tuning curve is believable.

In our collinear OPA, the conversion efficiency should be improved. The conversion efficiency of the OPA is mostly about 20%. During the constructional process, I think that the spatial overlap (spot size) and the pump duration can increase the conversion efficiency. Since the pump of 50fs is used as the pumping source, the pump of 100fs may have the better result according to this paper [11]. For the spatial overlap, we change the combination and specification of some lenses of the system to make the interacted spot size same. Additionally, there are two parameters that may have some influences; the  $\phi$  angle of the nonlinear crystal is not cut to zero degree and the backward beam (second stage) has a small angle with respect to the forward beam (the signal of the first stage).

$\theta_1 = 266^\circ 25'$  (phase matching angle  $24^\circ 7'$ )

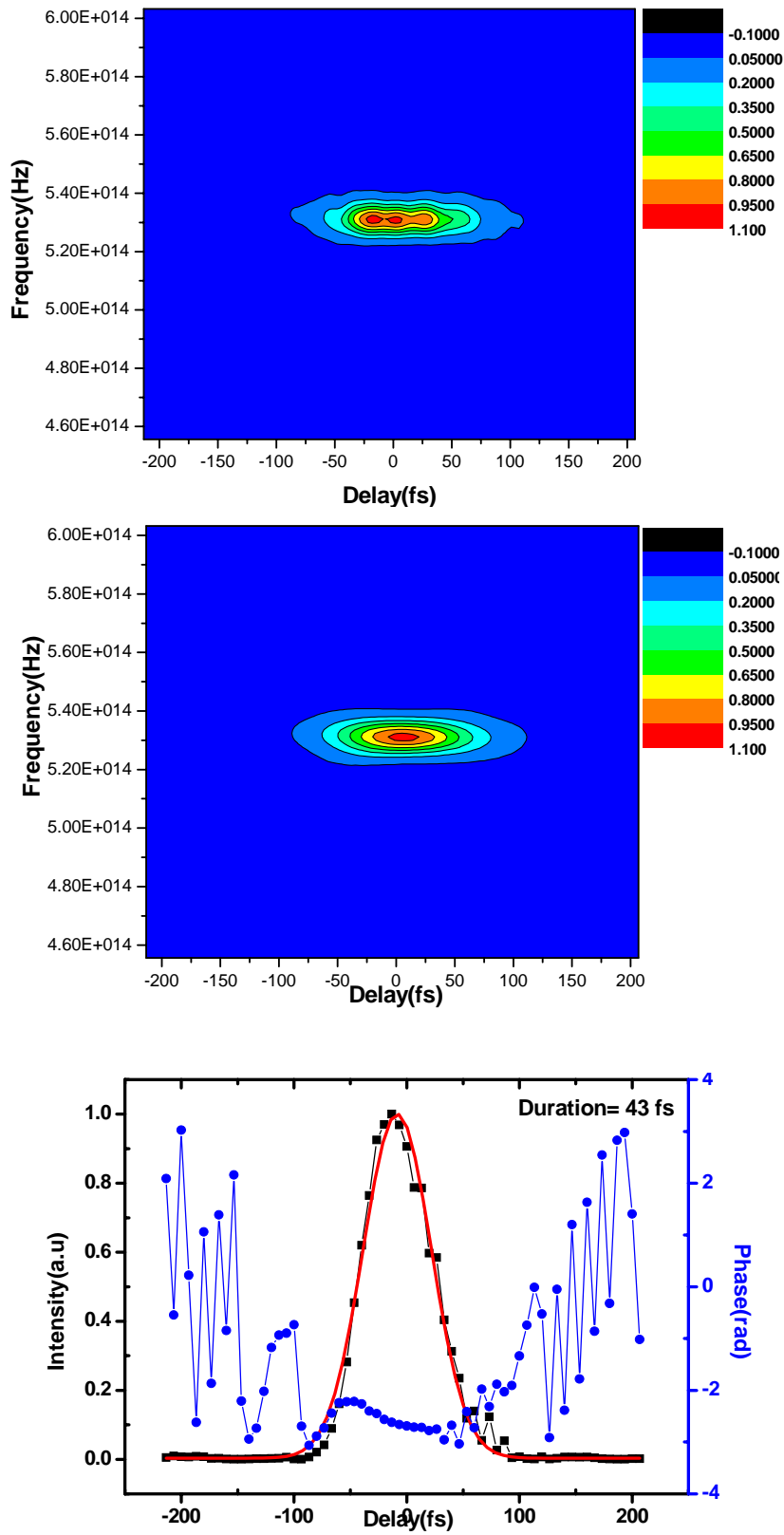


Fig. 3-6(a) Real Pattern; (b) Retrieved Pattern; (c) Electric field and phase

$\alpha_2 = 265^\circ 20'$  (phase matching angle  $25^\circ 8'$ )

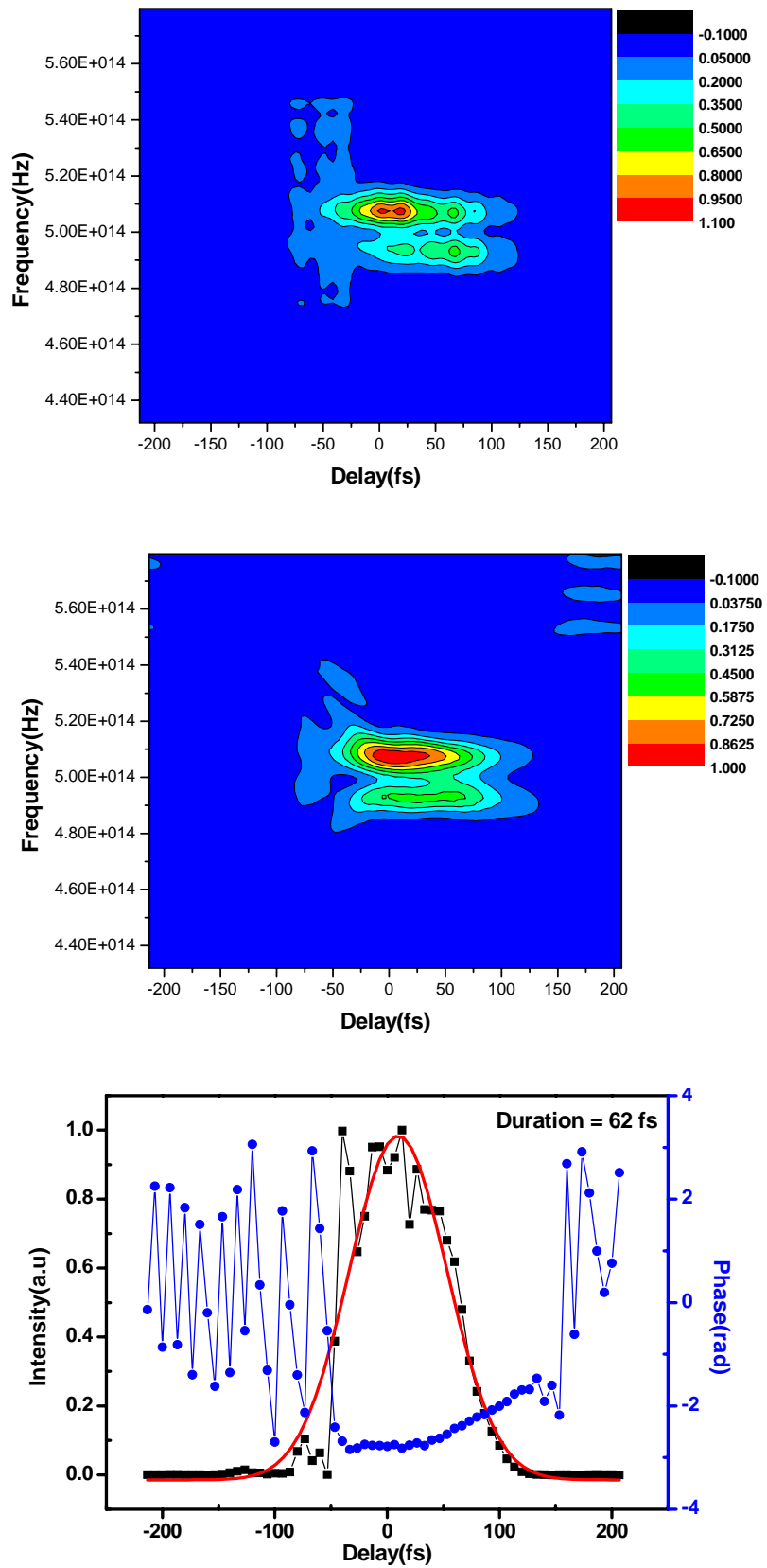


Fig. 3-7(a) Real Pattern; (b) Retrieved Pattern; (c) Electric field and phase

$\theta_3 = 264^\circ 40'$  (phase matching angle  $26^\circ 4'$ )

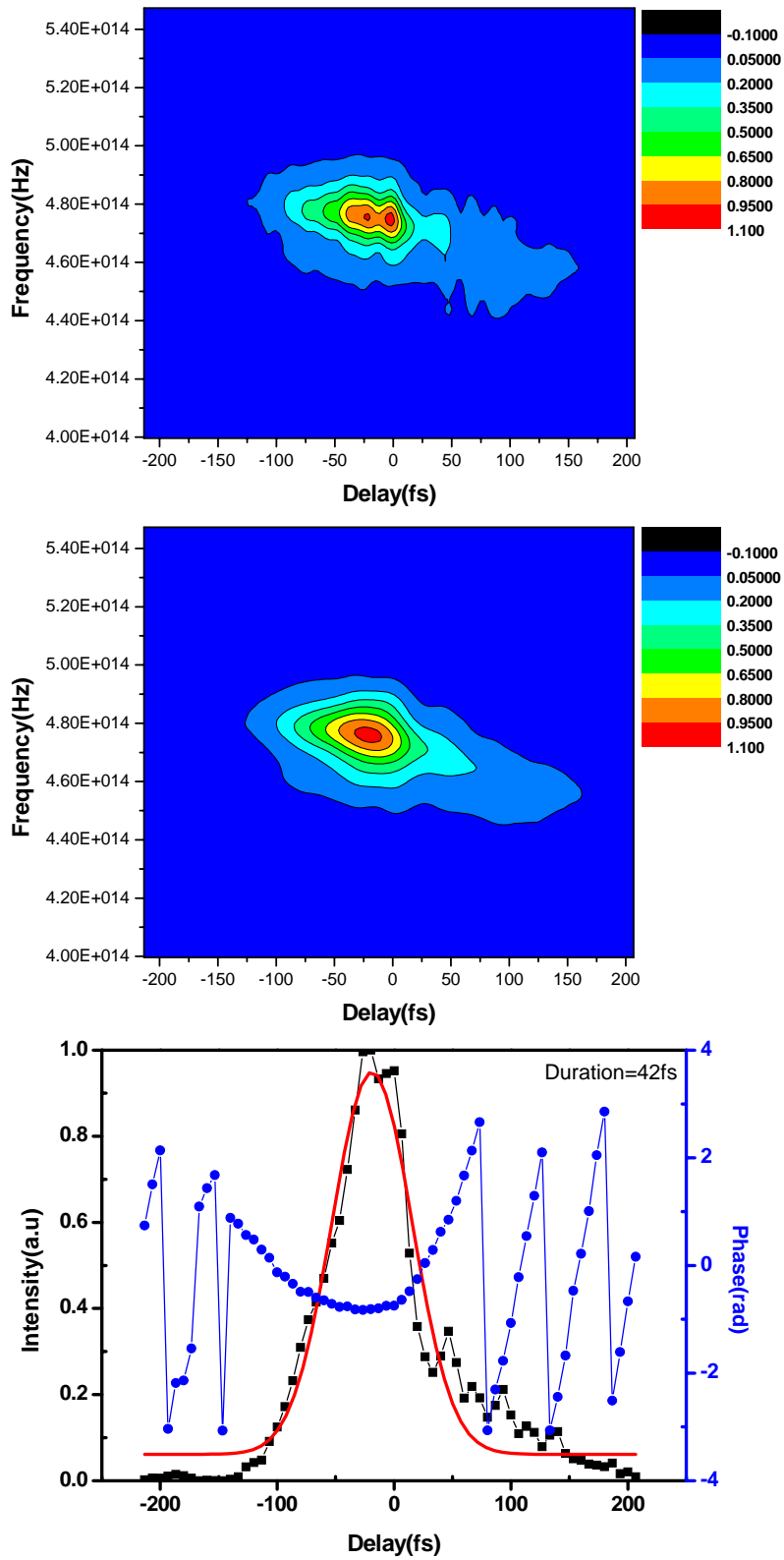


Fig. 3-8(a) Real Pattern; (b) Retrieved Pattern; (c) Electric field and phase

$\theta_4 = 263^\circ 45'$  (phase matching angle  $27^\circ 3'$ )

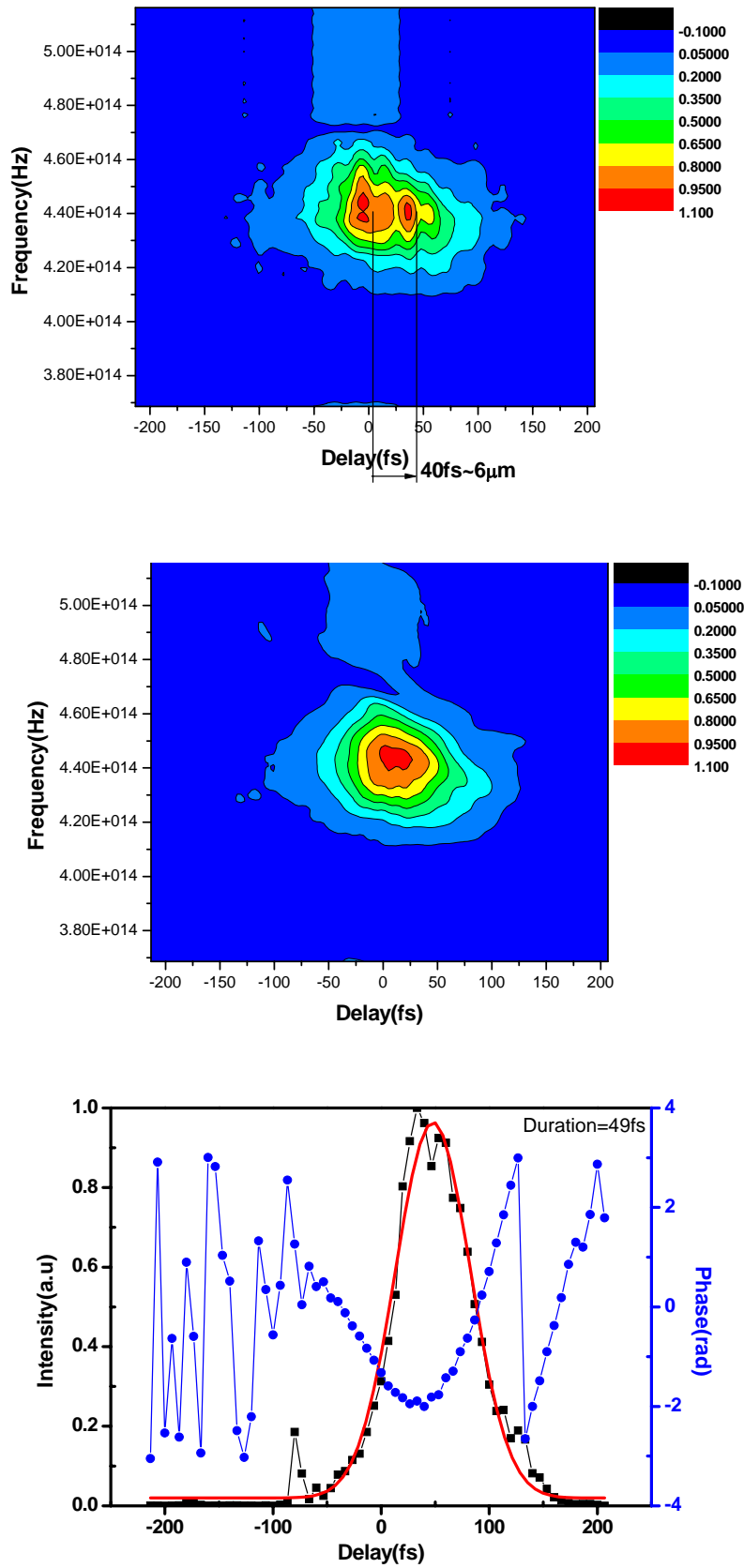


Fig. 3-9(a) Real Pattern; (b) Retrieved Pattern; (c) Electric field and phase

$\theta_4 = 263^\circ 25'$  (phase matching angle  $27^\circ 6'$ )

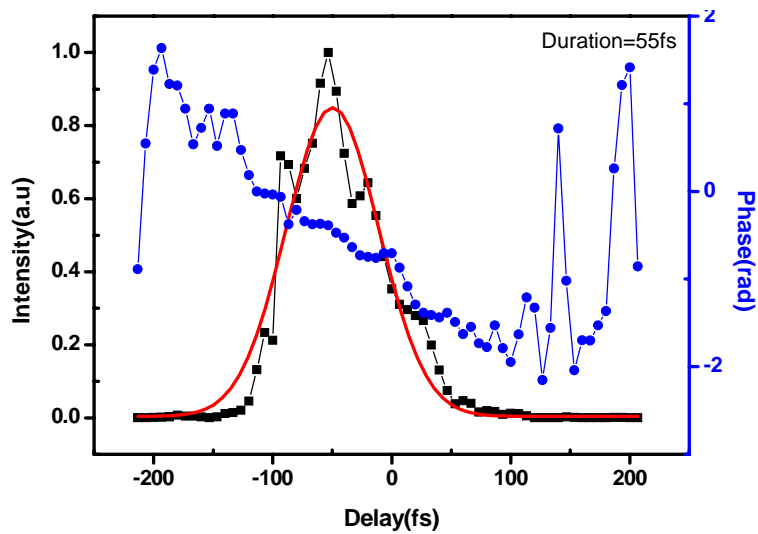
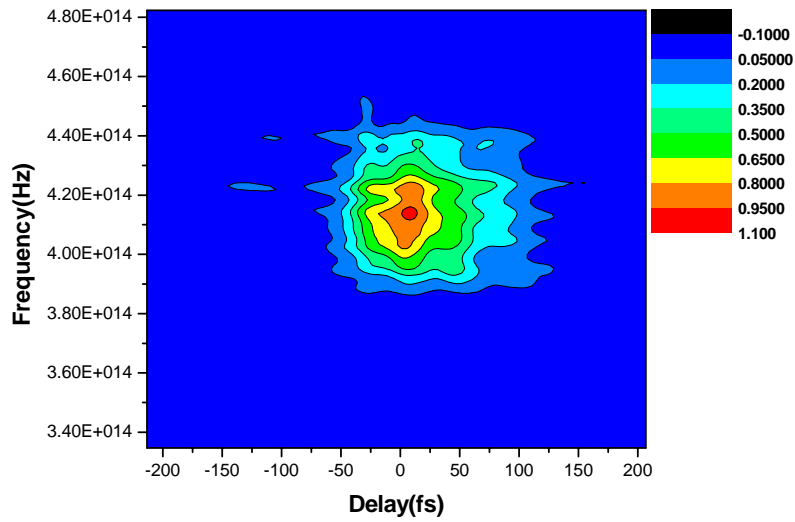
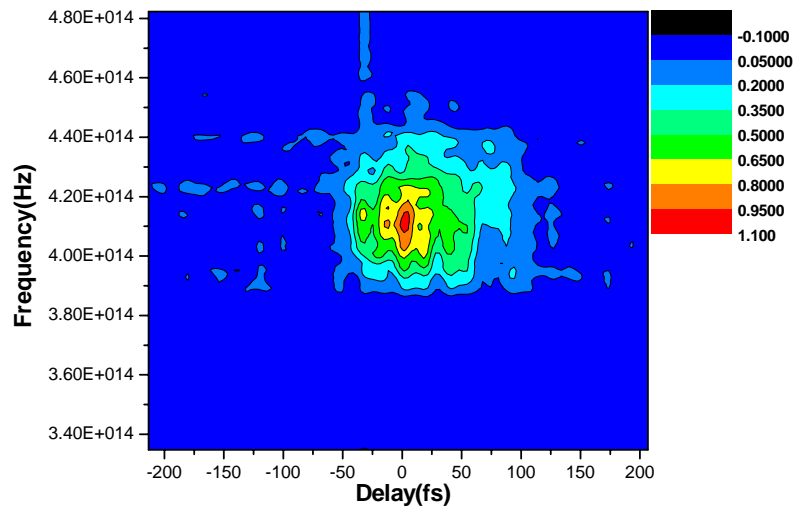


Fig. 3-10(a)Real Pattern; (b)Retrieved Pattern; (c)Electric field and phase

Wavelength(nm)	1141	1227	1294	1447	1524
PM angle(deg)	24.7°	25.8°	26.4°	27.3°	27.6°
PM angle of theory(deg)	25.0°	25.5°	26.0°	27.4°	28.1°
Bandwidth(nm)	52	117	145	46	66
Transform Limit(fs)	37	19	17	67	53
Measured Duration(fs)	43	62	42	49	55
Average Power (mW)	18	44	54	45	28

Table 3-1 The summary characterizations of the collinear OPA

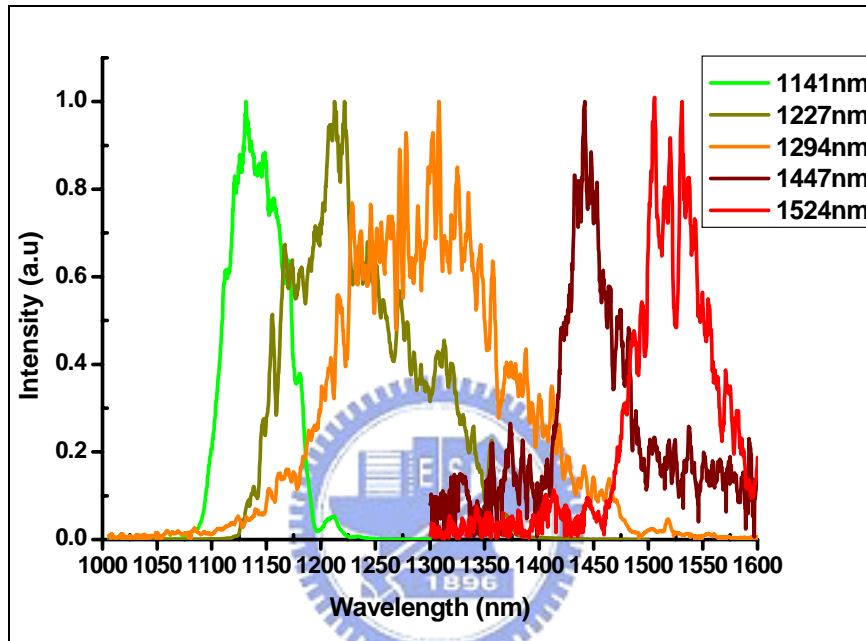


Fig. 3-11 The spectrum of the collinear OPA

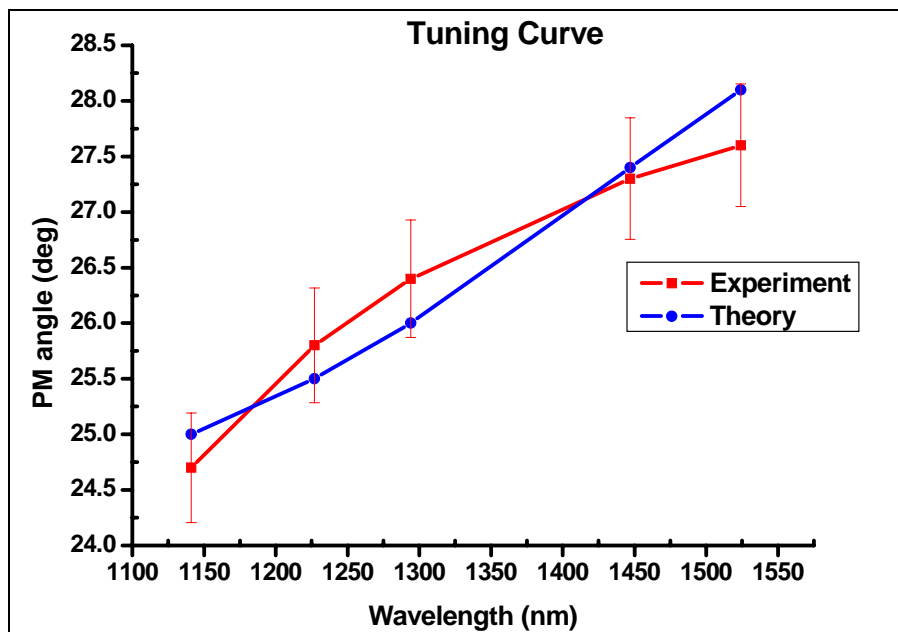


Fig. 3-12 The tuning range of the collinear OPA

# Chapter IV White Light Optical Parametric Amplifiers

## 4.1 Experimental system configuration

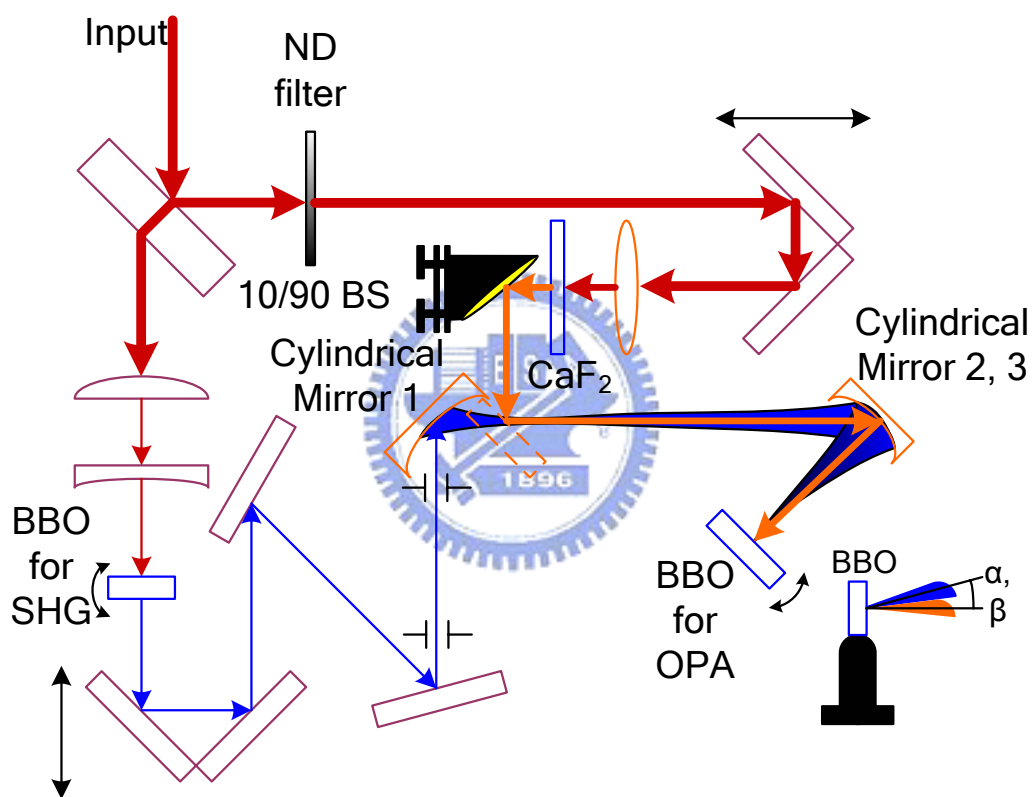


Fig. 4-1 The configuration of the white light OPA

In this part, the configuration of the white light OPA system is drawn in Fig. 4-1. The input is the same as the collinear type-II OPA. A small part of the input is split from the (10/90) beam splitter to generate the white light continuum using a CaF<sub>2</sub>. Then, the white light is collimated by a parabolic mirror and is focusing into the BBO (type I, z-cut at 29°) crystal by the cylindrical mirror. The remaining pulse energy of the pump



laser after a telescope generates the SHG (400nm) using a BBO crystal. The energy of the blue light is about 60  $\mu$ J. The spot size of the blue light is lengthened by a cylindrical mirror with short focal length. Then, the focused blue light by a cylindrical mirror with longer focal length interacts in the BBO crystal with white light seeding. The following figure is the actual configuration about this system.

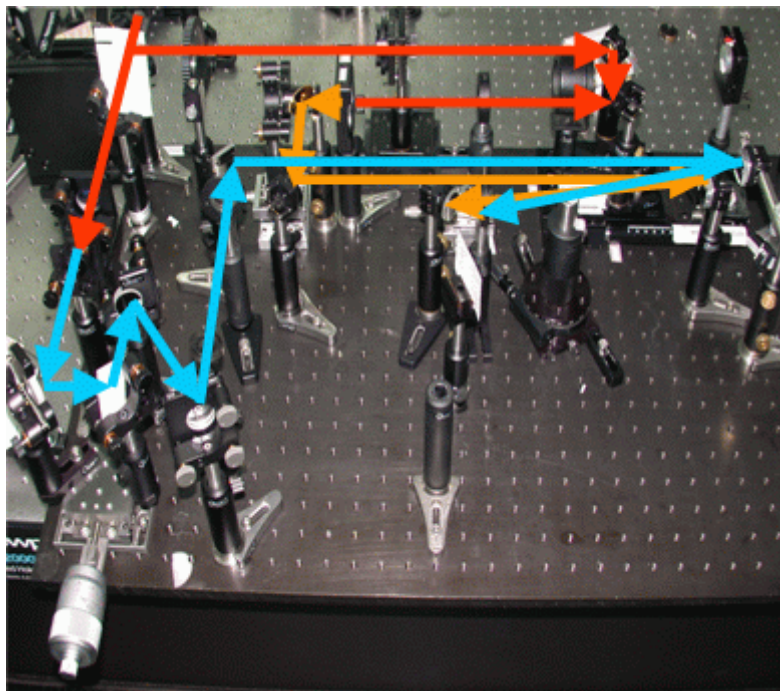


Fig. 4-2 The actual configuration of the white light OPA

## 4.2 Result of the White Light Optical Parametric Amplifiers

### 4.2.1 Tuning Range at Various $\alpha$ Angle

The configuration of the system is the same as shown in Fig. 4-1. The cylindrical mirror 1 replaces with a mirror and the spherical mirrors are used instead of the cylindrical mirror 2, 3. The geometry of the nonlinear crystal is the same as the above description but for  $\beta=0^\circ$ . We change the various  $\alpha$  and optimize the spatial overlap. We observe the spectrum after tuning the angle between the signal and the optical axis and optimizing the temporal overlap. The range of  $\alpha$  is determined by the spatial limitation and whether the OPA takes place or not.

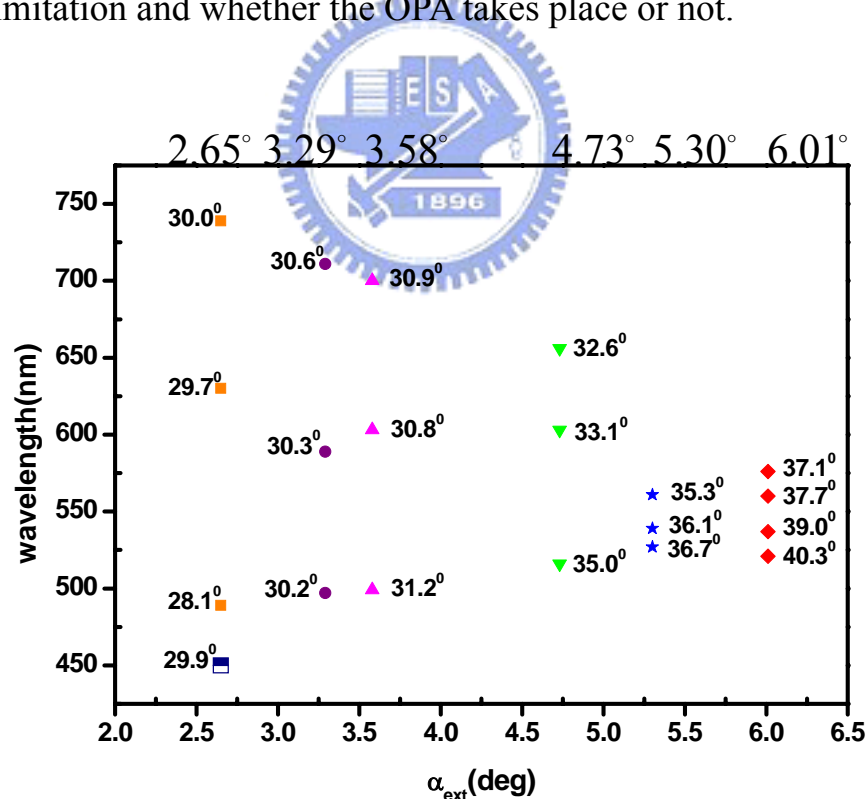
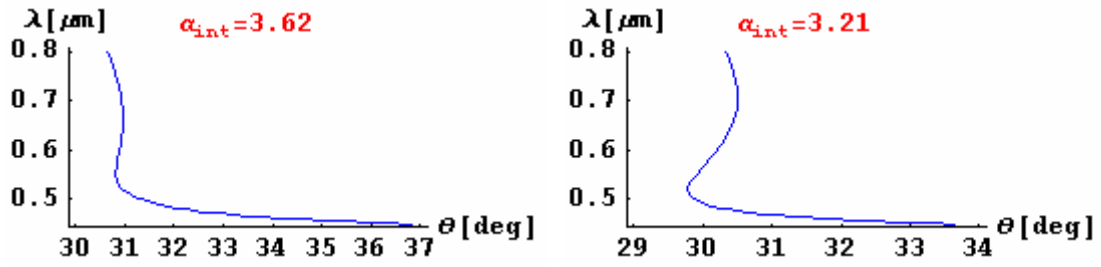


Fig. 4-3 Tuning range at various  $\alpha$  angles

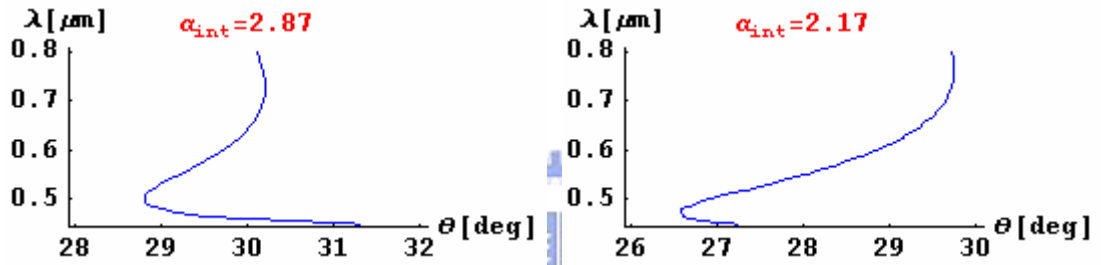
From the result as shown in Fig. 4-3, when the angle  $\alpha$  between the pump and the signal is small, the tuning range has the larger region than one of the large  $\alpha$ . For the large  $\alpha$ , the range is limited in some region about 550nm. When  $\alpha_{ext} = 2.65^\circ$  and the wavelength is tuned to 739nm, there is the other light with wavelength of 450nm simultaneously. At  $\alpha_{ext} = 5.30^\circ$ , the tuning range does not match the trend because the spatial overlap may be not optimized. To study the mechanism, we simulate and compare the phase matching curve at various  $\alpha$  angles. The simulation result is shown as Fig. 4-4.

When the  $\alpha$  angle is large, the phase matching angle also becomes large from the simulation result. Although the large phase matching angle influences the conversion efficiency, there should be the amplified light. Besides, the large included angle does reduce the effective nonlinear coefficient and the gain under this condition can not be too high. But, the short wavelength is still amplified due to the larger figure of merit (proportional to the reciprocal wavelength). Observe the collinear optical parametric amplification, the tuning range is quite broad. So, the tuning range is limited by the large included angle.

(a)  $\alpha_{ext} = 6.01^\circ$  ( $\alpha_{int} = 3.62^\circ$ ) (b)  $\alpha_{ext} = 5.30^\circ$  ( $\alpha_{int} = 3.21^\circ$ )



(c)  $\alpha_{ext} = 4.73^\circ$  ( $\alpha_{int} = 2.87^\circ$ ) (c)  $\alpha_{ext} = 3.58^\circ$  ( $\alpha_{int} = 2.17^\circ$ )



(e)  $\alpha_{ext} = 3.29^\circ$  ( $\alpha_{int} = 1.99^\circ$ ) (f)  $\alpha_{ext} = 2.65^\circ$  ( $\alpha_{int} = 1.61^\circ$ )

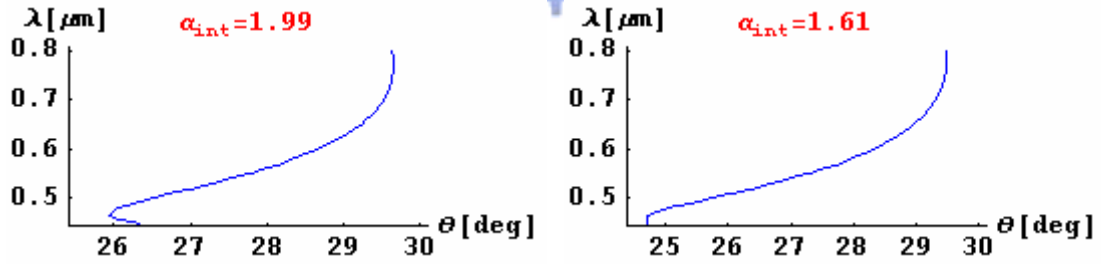


Fig. 4-4 (a)-(f) The phase-matching curve at various  $\alpha$  angles

## 4.2.2 Verifying the feasibility of white light OPA

Before studying the parameters of WL OPA, we make sure of the feasibility of WL OPA by the following experiment. First, we compare the bandwidth of WL OPA and NOPA, shown as Fig. 4-5. From the result, the bandwidth of WL OPA is really broader than one of NOPA. Then, we test the influence of the multi-beam pump geometric issue. We block a part of the lengthened pump by using a strip of thin paper; in other words, a part of  $\beta$  angles of the pump do not pump the BBO crystal. If the phase-matching curve is right, some wavelengths can not be amplified. Fig. 4-6 shows the complete spectrum and the blocked spectrum with several spot sizes. The wavelengths from 500nm to 700nm in the blocked spectrum of Fig. 4-6(a) do not be amplified in WL OPA. The same condition takes place in other spot sizes, seeing the Fig. 4-6(b) and (c). From these experiments, we can make sure that WL OPA really has the broader bandwidth and the effect of the geometric issues is the same as the expected one

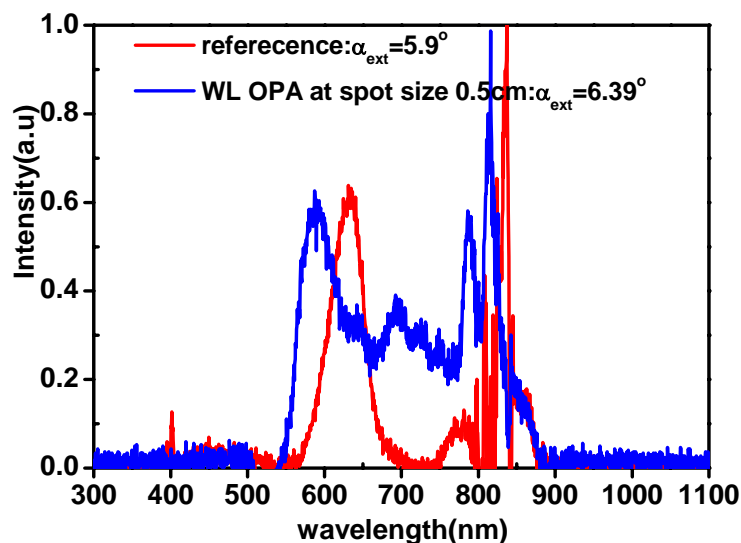
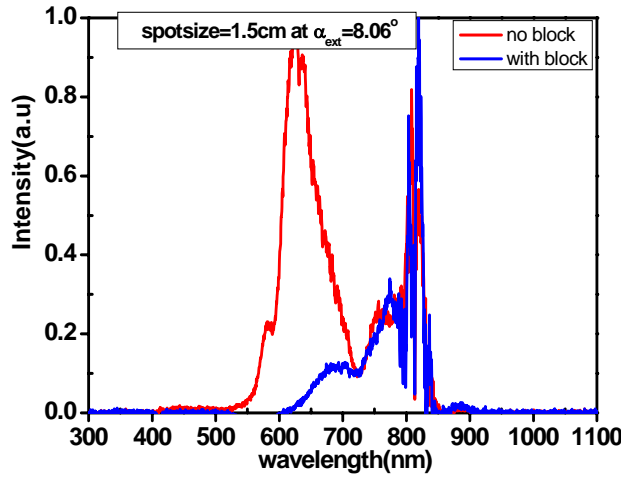
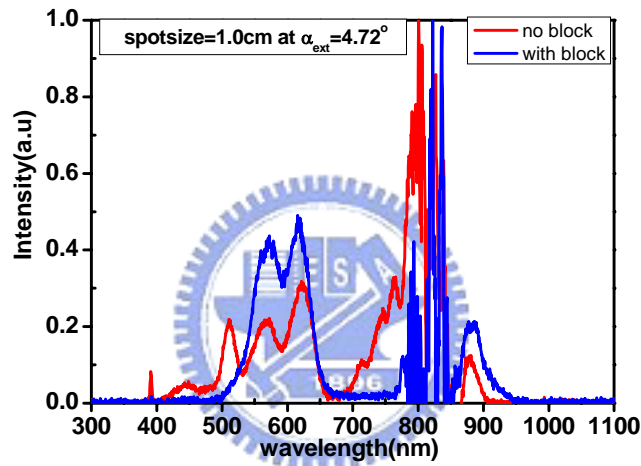


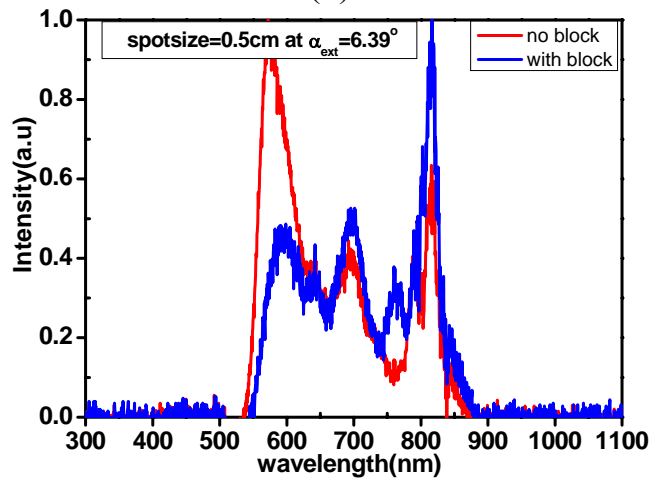
Fig. 4-5 The spectrum of WL OPA and NOPA



(a)



(b)



(c)

Fig. 4-6 The spectrum of the OPA and the blocked WL OPA. (a) spot size=1.5cm at  $\alpha_{\text{ext}}=8.06$  degree; (b) spot size=1.0cm at  $\alpha_{\text{ext}}=4.72$  degree; (c) spot size=0.5cm at  $\alpha_{\text{ext}}=6.39$  degree;

### 4.2.3 Studying the effect of various parameters

**Delay:** observe the effect of various delays at different spot sizes.

Fig. 4-7 (a)-(b) show the spectrums of various delays at  $\alpha_{\text{ext}}=3.66$ , 10.68 degree for spot size 1.5 cm. The induced delay due to the single shot geometric issue (acceptive delay) may be not enough at small  $\alpha$  angle. Therefore, the tunable range of the delay is limited as shown in Fig. 4-7(a). But for the large  $\alpha$  angle, there is the same situation, seeing the Fig. 4-7(c). Fig. 4-8 shows the phase matching curve of two  $\alpha$  angles ( $\alpha_{\text{ext}}=8.06$ , 10.68 degree at  $\theta_s=35$  degree). As shown Fig. 4-8, the wavelength range of large  $\alpha$  angle is smaller than one of small  $\alpha$  angle. In large  $\alpha$  angle, the acceptive delay is large but its wavelength range is limited. Therefore, the tunable range of large  $\alpha$  angle could not be large, seeing the Fig. 4-7(c). When the  $\alpha$  angle is a suitable angle, the acceptive delay is enough large to induce OPG of adjacent wavelength as shown in Fig. 4-9. The phenomenon in the spot size 1.0cm is the same as one in the spot size 1.5cm, seeing the Fig. 4-10(a)-(c).

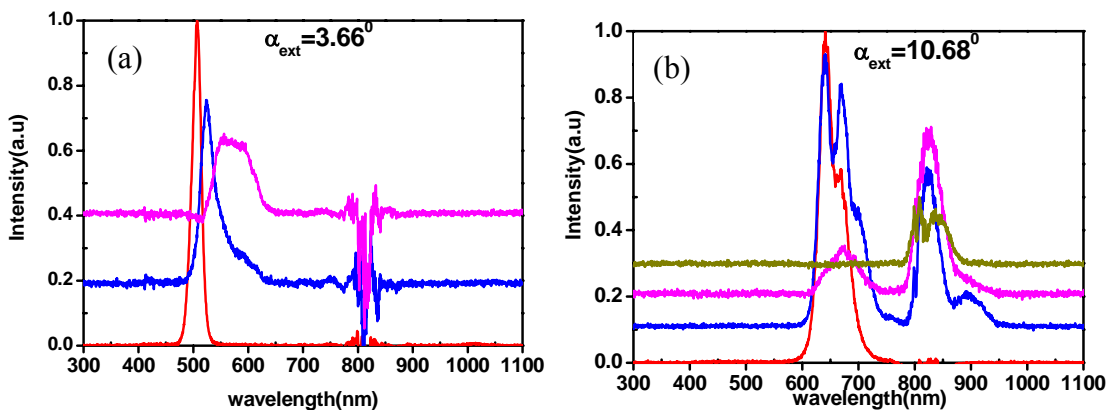


Fig. 4-7(a)-(b) The spectrums of various delays at  $\alpha_{\text{ext}}=3.66$ , 10.68 degree for spot size 1.5cm

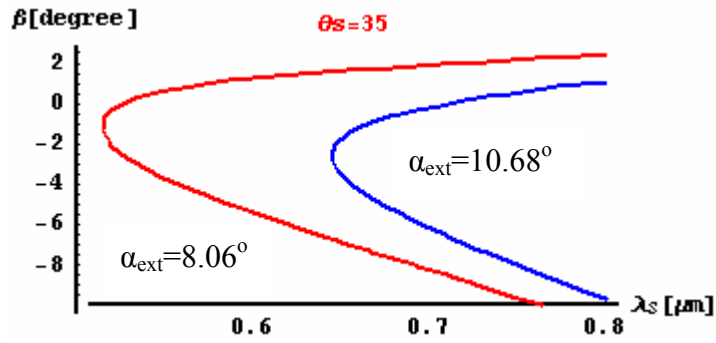


Fig. 4-8 The phase matching curve of two  $\alpha$  angles ( $\alpha_{\text{ext}}=8.06, 10.68$  degree at  $\theta_s=35$  degree)

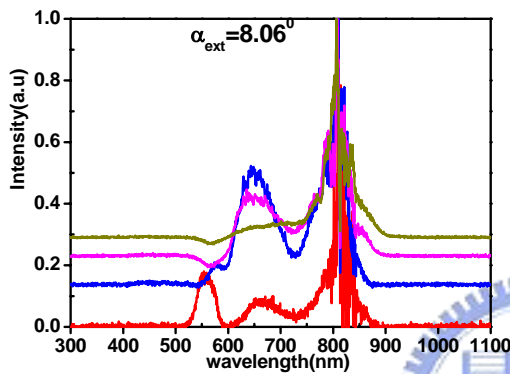


Fig. 4-9 The spectrums of various delays at  $\alpha_{\text{ext}}=8.06$  degree for spot size 1.5cm

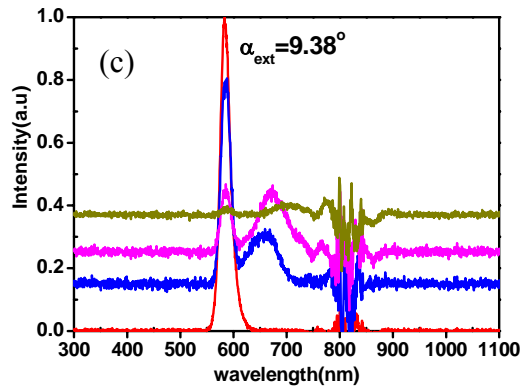
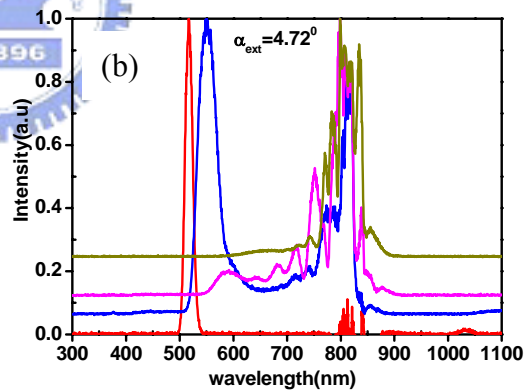
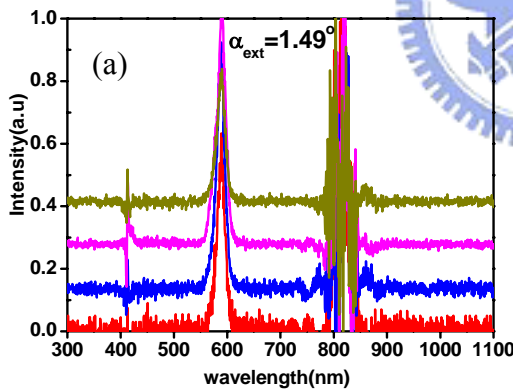


Fig. 4-9(a)-(c) The spectrums of various delays at  $\alpha_{\text{ext}}=1.49, 4.72, 9.38$  degree for spot size 1.0cm



**Spot Size:** observe the bandwidth of various spot sizes

As shown in Fig. 4-10, the first spectrum (1) has the broadest bandwidth among the three spectrums. Table 4-1 lists the experimental parameters. The result could be explained from its phase matching curve. The large spot size also indicates that the pump beam could pump the BBO crystal at more  $\beta$  angles. In other words, more wavelengths could satisfy the phase matching condition. When the pump beam becomes wider, the spectrum has a dip about 700nm. The wavelength of 700nm satisfies the phase matching condition at large  $\beta$  angles, seeing the phase matching curve (Fig. 4-11(a)). Fig. 4-11(b) shows the diagram of  $\beta$  distribution of the pump beam and the location of wavelength of 700nm ( $\Delta k=0$ ). As plot in Fig. 4-11(b), the wavelength of 700nm could be amplified at the side of the pump beam. Since the pump beam is spatially Gaussian distribution, the intensity of the side of the pump beam is weaker than the one of the central beam. The dip about 700nm could result from the decrement of the intensity of the pump beam. The phenomena are not obvious at small spot size.

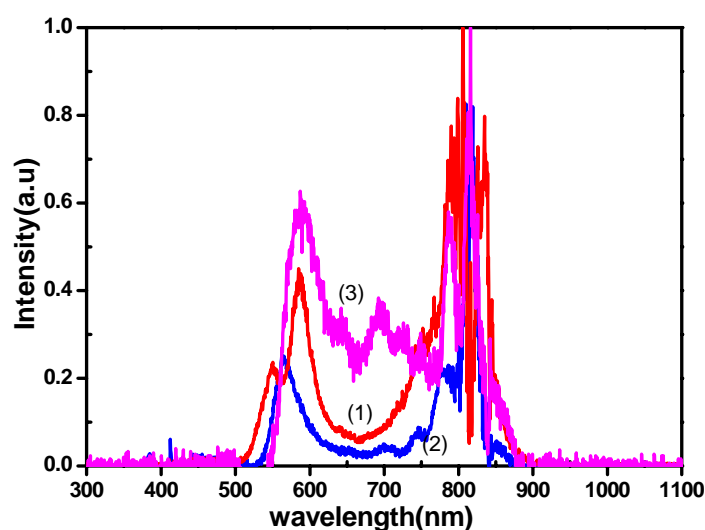


Fig. 4-10 Spectrum for various spot sizes

	(1)	(2)	(3)
Spot Size (cm)	1.5	1.0	0.5
$\alpha_{\text{ext}}$ (degree)	6.18	5.96	6.39

Table 4-1 The experimental parameters for the bandwidth of various spot size

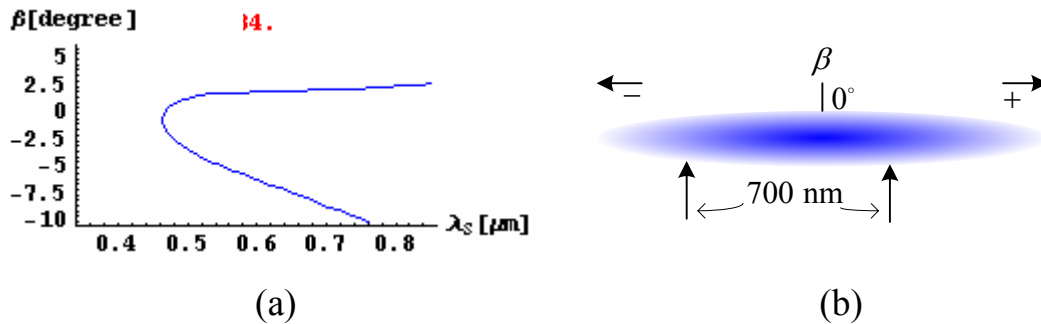


Fig. 4-11 (a) Phase matching curve at  $\theta=34^\circ$  and  $\alpha_{\text{int}}=3.7^\circ$ ; (b) A diagram of the pump beam ( $\beta$  distribution) and the location of wavelength of 700nm ( $\Delta k=0$ )



**Optical angle:** studying the effect during changing the optical angle

In the common collinear OPA, to rotate the optical angle is to tune the central wavelength. For the white light OPA, the wavelength of the peak is tuned by rotating the optical angle as shown in Fig. 4-12. But when the wavelength of  $\beta=0^\circ$  is moved to the long wavelength ( $\sim 700\text{nm}$ ), the short wavelength could not be amplified. Fig. 4-13 shows the phase matching curve at two optical angles. As plot in Fig. 4-13, the pulses with broad bandwidth could be generated if the wavelength of  $\beta=0^\circ$  moves to the short wavelength ( $\sim 500\text{nm}$ ).

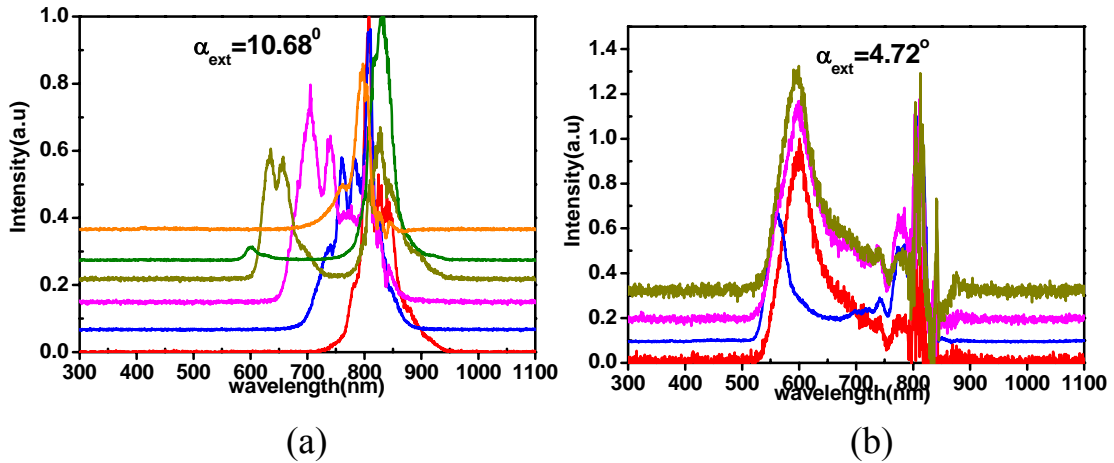


Fig. 4-12 (a) the spectrums of various optical angles at spot size 1.5cm and  $\alpha_{\text{ext}}=10.68^\circ$ ; (b) same as (a) but at spot size 1.0cm and  $\alpha_{\text{ext}}=4.72^\circ$

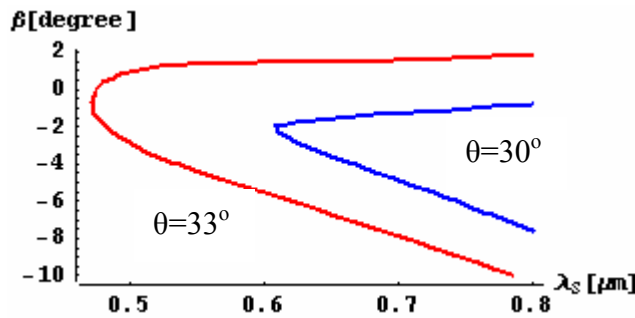


Fig. 4-13 Phase matching curves at two optical angles

## Whit Light OPA

Finally, we generate the pulses with broad bandwidth over 250nm at spot size 1.0cm and  $\alpha_{\text{ext}}=4.72^\circ$ , seeing the Fig. 4-14.

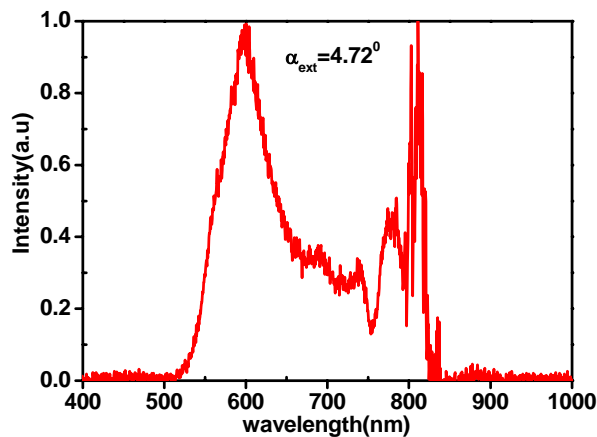


Fig. 4-14 Spectrum at spot size 1.0cm and  $\alpha_{\text{ext}}=4.72^\circ$

# Chapter IV Conclusion

## 5.1 Summary of this work

In this thesis, we construct a collinear type-II optical parametric amplifier. Its characteristics are (1) tuning range:  $\sim 1141\text{-}1524\text{nm}$  (expected idler:  $\sim 1687\text{-}2677\text{nm}$ ); (2) power:  $\sim 20\text{-}50\text{mW}$ ; (3) pulse width:  $\sim 50\text{-}60\text{fs}$ . The conversion efficiency (only  $\sim 10\%$ ) is not better than one of the typical OPA ( $\sim 20\text{-}30\%$ ) due to spatial overlap and duration of the pump beam. If the duration of the pump beam is  $100\text{ fs}$ , the conversion efficiency should be increased according to the simulation of the reference [11]. And, the spatial overlap of the pump beam and the signal is not optimized including the spot size and the alignment.

We try to study the mechanism of the white light optical parametric amplifier. We block some portion of the pump beam by using a strip of thin paper. Then, we observe some wavelength of the spectrum disappear. From it, the pump beam seems as the multi beam to pump a nonlinear crystal. Due to the single-shot geometric scheme, there is larger acceptance delay to let the various wavelengths be amplified simultaneously. Therefore, the pulses with the broad bandwidth over  $300\text{nm}$  could be generated by white light OPA. The duration of  $3\text{fs}$  could be expected after the suitable compression setup, such as the micromachined flexible mirror [12].

## 5.2 Future Directions

In the collinear type-II OPA, we could improve the spatial overlap in the second stage amplifier and find the suitable pulse width of the pump beam to increase the conversion efficiency. The average power of the OPA output could be over 100mW. For the white light OPA, it is expected to generate the pulse with the flat and broad bandwidth by amending the geometries and some parameters. Further, the pulse could be compressed by using the suitable compressor, such as double chirped mirror, flexible mirror and so on.



## Reference

[1] Jing-yuan Zhang, Jung Y. Huang and Y.R. Shen, "Optical Parametric Generation and Amplification," *Harwood Academic Publishers, United States*, 1995

[2] G. Cerullo, M. Nisoli, S. Stagira, and S. De Silvestri, "Sub-8-fs pulses from an ultrabroadband optical parametric amplifier in the visible," *Optics Letters*, vol 23, no 16, pp 1283-1285, August 1998

[3] A. Shirakawa, I. Sakane, M. Takasaka and T. Kobayashi, "Sub-5-fs visible pulse generation by pulse-front-matched noncollinear optical parametric amplification," *APL*, vol 74, no 16, pp 2268-2270, April 1999

[4] T. Kobayashi, and A. Shirakawa, "Tunable visible and near-infrared pulse generator in a 5 fs regime," *Appl. Phy. B*, vol 70, s239-s246, 2000

[5] Zeromskis E, A. Dubietis, G. Tamo\_sauskas and A. Piskarskas  
"Gain bandwidth broadening of the continuum-seeded optical parametric amplifier by use of two pump beams," *Optics Communications*, vol 203, pp 435-440, 2002

[6] Gunnar Arisholm, "Ultra-broadband chirped-pulse optical parametric amplifier with angularly dispersed beams," *OPTICS EXPRESS*, vol 12, no 3, pp 518-530, February 2004

[7] Rick Trebino, "Frequency-resolved optical gating: the measurement of ultrashort laser pulses," *Kluwer Academic Publishers, Boston*, 2000

[8] F. J. Duarte, "Tunable Lasers Handbook," *Academic Press, San Diego*, 1995.

[9] Giulio Cerullo and Sandro De Silvestri, "Ultrafast optical parametric amplifiers," *Rev. Sci. Instrum*, vol 74, no 1, pp 1-18, January 2003

[10] Rick Trebino, "Frequency-resolved optical gating: the measurement of ultrashort laser pulses," *Kluwer Academic Publishers, Boston*, 2000

[11] D. Pang, Ruobing Zhang and Qingyue Wang, “Theoretical analysis of noncollinear phase-matched optical parametric amplifier seeded by a white light continuum,” *Optics Communications*, vol 196, pp 293-298, 2001

[12] Andrius Baltuška, “Visible pulse compression to 4 fs by optical parametric amplification and programmable dispersion control,” *Optical Letters*, vol 27, no 5, pp 306-308, March 2002

